

The Construction and Application of Penrose Diagrams, with a Focus on the Maximally Analytically Extended Schwarzschild Spacetime

Christian Röken^{1,2,*}

¹*Argelander Institute for Astronomy - University of Bonn, 53121 Bonn, Germany*

²*Lichtenberg Group for History and Philosophy of Physics - Faculty of Philosophy, University of Bonn, 53113 Bonn, Germany*

(Dated: July 2025)

ABSTRACT. We present a detailed, mathematically rigorous description of the construction procedure of Penrose diagrams for the example of the maximal analytic extension of the exterior Schwarzschild spacetime. To this end, we first outline the basic idea underlying Penrose diagrams, state the general requirements on the spacetimes to be visualized, and give a definition of Penrose diagrams. We then construct the Penrose diagram of the maximally analytically extended Schwarzschild spacetime and discuss the characteristics and properties corresponding to this particular Penrose diagram. As an application, we work out the differences between the spacetime and null variants of the canonical advanced Eddington–Finkelstein coordinate representations of the exterior Schwarzschild spacetime by explicitly constructing and visually analyzing Penrose diagrams equipped with foliations of the level sets of the respective Eddington–Finkelstein time and null coordinates. Throughout the course of the paper, we provide brief accounts of the relevant parts of the seminal publications on the exterior Schwarzschild solution by Schwarzschild himself, Kruskal, Eddington, Finkelstein, and Penrose. This paper is primarily of pedagogical nature aimed at graduate students in physics and applied mathematics (with a background in general relativity and differential geometry), serving mainly as an introduction to Penrose diagrams and coordinate representations of the exterior Schwarzschild spacetime.

Contents

I. Introduction	2
II. Preliminaries	2
A. Historical Remarks on the Exterior Schwarzschild Solution	2
B. Modern Account of the Exterior Schwarzschild Solution and Kruskal’s Maximal Analytic Extension	6
III. Basic Idea Behind Penrose Diagrams	8
IV. Construction Procedure of the Penrose Diagram of the Maximally Analytically Extended Schwarzschild Spacetime	9
A. Coordinate Representation for the Penrose Diagram	9
B. Components of the Penrose Diagram	14
V. Application to Eddington–Finkelstein and Penrose Foliations	16
A. Historical Remarks on the Eddington–Finkelstein and Penrose Representations of the Exterior Schwarzschild Solution	17
1. Eddington–Finkelstein Coordinates	17
2. Penrose Coordinates	20
B. Comparison of Eddington–Finkelstein and Penrose Foliations	21
Acknowledgments	23
References	23

*Electronic address: croeken@uni-bonn.de

I. INTRODUCTION

In the framework of general relativity, and more generally in the field of differential geometry, many questions of interest are concerned with the global causal structure and the infinities of 4-dimensional curved spacetimes. A particularly useful visualization tool in this regard are Penrose diagrams, which are faithful 2-dimensional, finite-sized diagrammatic representations that contain the determining information on the global causal structure and on possible infinities of entire (or certain subsets of) 4-dimensional spacetimes. The general idea underlying Penrose diagrams was first introduced by Roger Penrose in 1963/64 in [32, 33] and developed further into its present-day form by Carter and Walker in [2] and [43], respectively. Penrose diagrams may be considered as the natural finite-sized, non-Minkowskian extension of the usual Minkowski diagrams of special relativity or a finite-sized variant of the standard Kruskal diagrams of general relativity, where infinity is now on the boundary of the diagram, which allows for proper studies of asymptotic properties of spacetimes.

The aim of this paper is to give a comprehensive pedagogical but at the same time mathematically rigorous account of Penrose diagrams for graduate students in physics and applied mathematics having a solid background in general relativity and differential geometry,¹ viz., we discuss the general idea behind—and the conditions for—Penrose diagrams, their construction procedure, their characteristics and properties, and lastly a possible application. For the latter, we address how Penrose diagrams can be used to illustrate, and thus identify, differences between different coordinate representations of spacetimes, in particular, the differences between the two variants of the canonical advanced Eddington–Finkelstein coordinate representations of the analytic extension of the exterior Schwarzschild spacetime across the future event horizon.

We shall proceed in the following way. In the preliminary section II A, we first recall the details and main results of Schwarzschild’s acclaimed 1916 paper [38] on the derivation of the external gravitational field of a massive point particle within the theory of general relativity before giving a modern account of this so-called exterior Schwarzschild solution and the construction of the corresponding maximal analytic extension, for which we recapitulate Kruskal’s 1960 paper [21], in Section II B. In Section III, we discuss the general idea at the basis of Penrose diagrams, formulate conditions on the spacetimes to be represented, specify the characteristics of Penrose diagrams, and then give a more rigorous definition of these diagrams. Subsequently, in Section IV, we get to a detailed conceptual step-by-step description of the construction procedure of Penrose diagrams, focusing on the maximally analytically extended Schwarzschild spacetime and the required coordinate representations. For an application of this Penrose diagram, we discuss in Section V A, on the one hand, the relevant parts pertaining to the spacetime variant of the advanced Eddington–Finkelstein coordinate representation of the exterior Schwarzschild solution introduced in Eddington’s 1924 paper [8] and Finkelstein’s 1958 paper [14], and, on the other hand, the details of the null variant employed in Penrose’s 1969 paper [35].² With this at hand, we finally answer the question of how precisely these two variants differ by visually analyzing—and then comparing the characteristics of—the families of level sets of the respective Eddington–Finkelstein time and Penrose null coordinates foliating the combined exterior and interior black hole regions of the Penrose diagram of the maximal analytic extension in Section V B.

II. PRELIMINARIES

A. Historical Remarks on the Exterior Schwarzschild Solution

In order to present the construction procedure of Penrose diagrams on the basis of the example of the maximally analytically extended Schwarzschild spacetime, we first briefly recall the relevant background of Schwarzschild’s original solution. In 1916, Karl Schwarzschild published two very influential papers, [38] and [39], on the gravitational field of spherically symmetric objects within the framework of Einstein’s then newly established theory of general relativity. To be more precise, the aim of the first of these papers, which is the relevant for the present study, was the derivation of an explicit analytical solution of the vacuum Einstein field equations that describes the gravitational field of an isolated, spherically symmetric point particle of invariant mass located at the origin of a Cartesian coordinate

¹ For basic introductions into general relativity and differential geometry see the standard textbooks [18, 26, 42] and [22, 28, 29], respectively.

² Here, we shall refer to the null variant of the advanced Eddington–Finkelstein coordinates, although coined “Eddington–Finkelstein coordinates” by Penrose himself, as “Penrose coordinates,” for they are sufficiently different in comparison to the coordinates used by Eddington and Finkelstein (for details see Section V A).

system $(x^i)_{i \in \{1,2,3\}} \in \mathbb{R}^3 \setminus \{\mathbf{0}\}$ for times $x^4 \in \mathbb{R}$, together covering a connected 4-manifold \mathfrak{M} , for the study of the movement of a test particle in such a gravitational field.^{3,4} To this end, Schwarzschild was seeking a metric \mathbf{g} that at every event satisfies the unimodularity condition $|\det(\mathbf{g})| = -1$ and the field equations

$$\partial_\alpha \Gamma_{\mu\nu}^\alpha + \Gamma_{\mu\beta}^\alpha \Gamma_{\nu\alpha}^\beta = 0, \quad (1)$$

where

$$\Gamma_{\mu\nu}^\alpha = -\frac{1}{2} g^{\alpha\beta} (\partial_\nu g_{\mu\beta} + \partial_\mu g_{\nu\beta} - \partial_\beta g_{\mu\nu})$$

are the usual Christoffel symbols of the second kind and $\mu, \nu \in \{1, 2, 3, 4\}$, while at the same time it is being subjected to the following conditions:

- (C1) All metric components $(g_{\mu\nu})_{\mu, \nu \in \{1,2,3,4\}}$ are independent of the time coordinate x^4 .
- (C2) The spatio-temporal metric components $(g_{i,4})_{i \in \{1,2,3\}}$ are identically zero.
- (C3) The metric is spatially symmetric around the origin in the sense that it is invariant under special orthogonal transformations $T \in SO(3)$ [i.e., rotations] applied to the coordinates $(x^i)_{i \in \{1,2,3\}}$.
- (C4) Except for the four diagonal metric components $(g_{\mu\mu})_{\mu \in \{1,2,3,4\}}$, which are assumed to tend to the constants $g_{11} = g_{22} = g_{33} = -g_{44} = -1$, all metric components vanish at infinity.

Conditions (C1) and (C2) together imply that the spacetime described by the metric \mathbf{g} is static,⁷ whereas Conditions (C3) and (C4) entail that it is spherically symmetric and asymptotically flat, respectively.⁸ Employing the notation $(x = x^1, y = x^2, z = x^3)$ and $t = x^4$, and the radial distance $r = \sqrt{x^2 + y^2 + z^2}$, Schwarzschild begins by making use of the metric ansatz

$$\mathbf{g} = F(r) dt \otimes dt - G(r) [dx \otimes dx + dy \otimes dy + dz \otimes dz] - H(r) [xdx + ydy + zdz] \otimes [xdx + ydy + zdz], \quad (2)$$

which satisfies all the above conditions assuming that at spatial infinity $F, G \rightarrow 1$ and $H \rightarrow 0$. In a next step, possibly for simplicity, he applies the transformation from Cartesian to spherical polar coordinates

$$\mathfrak{T}^{(1)}: \begin{cases} \mathbb{R} \setminus \{0\} \times \mathbb{R} \setminus \{0\} \times \mathbb{R} \setminus \{0\} \rightarrow \mathbb{R}_{>0} \times (0, \pi) \times [0, 2\pi) \\ (x, y, z) \mapsto (r, \vartheta, \phi) \end{cases} \quad (3)$$

with

$$\vartheta = \arccos\left(\frac{z}{\sqrt{x^2 + y^2 + z^2}}\right) \quad \text{and} \quad \phi = \text{sgn}(y) \left[\arccos\left(\frac{x}{\sqrt{x^2 + y^2}}\right) - \pi \right] + \pi.$$

³ For a historical overview of this paper see, e.g., [12, 13]. A comprehensive physical review can be found in [19].

⁴ The origin at $(x^1, x^2, x^3) = \mathbf{0}$, which is, according to Schwarzschild, the location of the field-generating point mass (cf. Remark II.3), is not contained in the range of the Cartesian coordinates, as for Schwarzschild only the gravitational field outside the point mass is of interest.

⁵ In fact, Schwarzschild employed the earlier unimodular vacuum Einstein field equations introduced in [9] instead of the fully covariant vacuum Einstein field equations defined in [10]. This, however, does not pose a problem for later analyses of the gravitational field of a point particle, as the resulting solution indeed satisfies both of these sets of equations. Schwarzschild's paper was followed shortly after by Droste's work [7] that more rigorously deals with the same problem within the generally covariant framework.

⁶ Schwarzschild himself did not specify any details of the underlying manifold \mathfrak{M} . Moreover, he gave no mathematical definition of the metric \mathbf{g} except for stating that it is "a function of the variables \mathbf{x} ," that is, of the spacetime coordinates. However, from a modern differential geometric point of view, the manifold may be considered as being smooth and the metric may be interpreted as a section of the tensor product bundle of the cotangent bundle $T^*\mathfrak{M}$ with itself, so that Schwarzschild was ultimately looking for solutions $\{\mathbf{g} \in \Gamma(\mathfrak{M}, T^*\mathfrak{M} \otimes T^*\mathfrak{M}) \mid |\det(\mathbf{g})| = -1\}$ of the unimodular Einstein field equations (1).

⁷ Staticity can, more properly, be inferred from the fact that the vector field ∂_{x^4} is a globally timelike and irrotational Killing field.

⁸ Mathematically more rigorously, spherical symmetry may be viewed as the special orthogonal group $SO(3)$ acting as the group of isometries $\mathfrak{I}: \mathfrak{M} \times SO(3) \rightarrow \mathfrak{M}$, where the set of fixed points $\mathfrak{I}((x^\mu)_{\mu \in \{1,2,3,4\}}, R) = (x^\mu)_{\mu \in \{1,2,3,4\}}$ for all $R \in SO(3)$ is a 1-dimensional timelike surface referred to as the *axis of symmetry*. Asymptotic flatness, on the other hand, simply means that at spacelike infinity the metric becomes Minkowskian, i.e., $\lim_{r \rightarrow \infty} \mathbf{g} = \boldsymbol{\eta} = dx^4 \otimes dx^4 - dx^1 \otimes dx^1 - dx^2 \otimes dx^2 - dx^3 \otimes dx^3$.

This transformation, however, gives rise to coordinates that are not unimodular as required by the field equations defined in Equation (1) [cf. Footnote 5]. To resolve this problem, Schwarzschild rewrites the spatial volume element represented in the spherical polar coordinates (3) in the form

$$\text{vol}_3 = r^2 \sin(\vartheta) dr d\vartheta d\phi = d\left(\frac{r^3}{3}\right) d(-\cos(\vartheta)) d\phi = dx_1 dx_2 dx_3,$$

which makes it possible to directly read out the transformation from spherical polar coordinates to unimodular spherical polar coordinates^{9,10}

$$\mathfrak{T}^{(2)}: \begin{cases} \mathbb{R}_{>0} \times (0, \pi) \times [0, 2\pi) \rightarrow \mathbb{R}_{>0} \times (-1, 1) \times [0, 2\pi) \\ (r, \vartheta, \phi) \mapsto (x_1, x_2, x_3) \end{cases}$$

with

$$x_1 = \frac{r^3}{3}, \quad x_2 = -\cos(\vartheta), \quad \text{and} \quad x_3 = \phi.$$

Expressed in these coordinates, the metric ansatz (2) becomes

$$\mathbf{g} = F(r) dx_4 \otimes dx_4 - \frac{1}{r^2} \left(\frac{G(r)}{r^2} + H(r) \right) dx_1 \otimes dx_1 - G(r) r^2 \left[\frac{dx_2 \otimes dx_2}{1 - x_2^2} + (1 - x_2^2) dx_3 \otimes dx_3 \right], \quad (4)$$

where the radial distance in unimodular spherical coordinates yields $r = (3x_1)^{1/3}$. Using the abbreviations $f_1 = r^{-2} [G/r^2 + H]$, $f_2 = f_3 = Gr^2$, and $f_4 = F$,¹¹ and inserting this ansatz into the Einstein field equations (1), Schwarzschild finds the solutions

$$f_1 = \frac{(3x_1 + \alpha^3)^{-1}}{[(3x_1 + \alpha^3)^{1/3} - \alpha]}, \quad f_2 = f_3 = (3x_1 + \alpha^3)^{2/3}, \quad \text{and} \quad f_4 = 1 - \frac{\alpha}{(3x_1 + \alpha^3)^{1/3}},$$

in which $\alpha \in \mathbb{R}_{>0}$ is a constant of integration. Finally, to further simplify the metric representation corresponding to these solutions, he employed the transformation from the unimodular spherical polar coordinates to what are today called Schwarzschild coordinates

$$\mathfrak{T}^{(3)}: \begin{cases} \mathbb{R}_{>0} \times (-1, 1) \times [0, 2\pi) \rightarrow (\alpha, \infty) \times (0, \pi) \times [0, 2\pi) \\ (x_1, x_2, x_3) \mapsto (R, \vartheta, \phi) \end{cases}$$

with

$$R = (3x_1 + \alpha^3)^{1/3}, \quad \vartheta = \pi - \arccos(x_2), \quad \text{and} \quad \phi = x_3.$$

This yields the familiar expression for the metric accounting for the gravitational field of a massive, spherically symmetric point particle

$$\mathbf{g} = \left[1 - \frac{\alpha}{R} \right] dt \otimes dt - \left[1 - \frac{\alpha}{R} \right]^{-1} dR \otimes dR - R^2 \mathbf{g}_{S^2}, \quad (5)$$

⁹ This is possible because of the particular product structure of the Jacobian determinant for the change from Cartesian to spherical polar coordinates.

¹⁰ Schwarzschild's unimodular spherical polar coordinates (x_1, x_2, x_3) must not be confused with the usual covariant form of his initially chosen Cartesian coordinates (x^1, x^2, x^3) .

¹¹ These new functions have to fulfill the following set of conditions:

1. In the limit $x_1 \rightarrow \infty$, $f_1 = r^{-4} = (3x_1)^{-4/3}$, $f_2 = f_3 = r^2 = (3x_1)^{2/3}$, and $f_4 = 1$.
2. The determinantal equation $f_1 f_2 f_3 f_4 = 1$ has to be satisfied.
3. (f_1, f_2, f_3, f_4) is an exact solution to the Einstein field equations.
4. All f_i , $i \in \{1, 2, 3, 4\}$, have to be continuous except at $x_1 = 0$.

where $g_{S^2} = d\vartheta \otimes d\vartheta + \sin^2(\vartheta) d\phi \otimes d\phi$ is the metric on the unit 2-sphere.¹²

Remark II.1. For the given choice of time coordinate t , the metric representation (5) is invariant under both time translations $t \mapsto t' = t + \text{const.}$ and time reversals $t \mapsto t' = -t$. Moreover, Schwarzschild's radial coordinate R , which is a generalized spherical polar-type coordinate that behaves like the usual spherical polar radial coordinate r only in the asymptotic end (i.e., for $R \rightarrow \infty$), has the property that each sphere $\{(t, R, \vartheta, \phi) \mid t, R = \text{const.}, \vartheta \in (0, \pi), \text{ and } \phi \in [0, 2\pi)\}$ has an intrinsic surface area of $4\pi R^2$. Radial coordinate transformations of type $R' = f(R) \in C^\infty(\mathbb{R})$ with $f(R) \rightarrow R$ as $R \rightarrow \infty$ preserve the general form of the metric. The same holds for rotational and reflective transformations of the angular coordinates (ϑ, ϕ) about the origin.

Remark II.2. The constant of integration α is later identified with the constant $2M$ (given in natural units), where $M \in \mathbb{R}_{>0}$ is the common Newtonian mass of a massive point particle. For this purpose, one usually takes the weak-field limit [that is $\alpha \ll (3x_1 + \alpha^3)^{1/3}$] of the geodesic equation of motion, making it concordant with Newton's laws of motion for a test particle moving in the Newtonian gravitational field generated by a massive point particle. Here, the weak-field limit applies for either movements at large distances from the gravitating source or for extremely light sources. This fixes the $g_{x_4 x_4}$ -component of the metric (4) to be $F = 1 - 2M/[r^3 + 8M^3]^{1/3}$. The parameter M can furthermore be shown to coincide with the ADM mass of the point mass source. In the limit $M \rightarrow 0$, one expectedly obtains the Minkowski metric expressed in unimodular spherical polar coordinates. Besides, for $M \in \mathbb{R}_{<0}$, the exterior Schwarzschild solution contains a naked singularity.

Remark II.3. By extending the Schwarzschild representation (5) of the exterior Schwarzschild solution across $R = \alpha$ into the nonstatic interior spacetime region with $\text{Ran}(R) = (0, \alpha)$, one finds, in addition to the in a limiting sense already existing coordinate singularity at $R = \alpha$, a curvature singularity at the location $R = 0$, which, however, corresponds to $r = -\alpha$, not coinciding with the by Schwarzschild originally assumed massive point particle location at $r = 0$. Accordingly, following the usual placeholder interpretation that identifies the gravitational-field-generating source with the curvature singularity at $R = 0$, implying the complete arbitrariness of coordinates, Schwarzschild assigning the location of the point particle to $r = 0$ in the first place was unfounded. Nevertheless, at that time, it was not yet known that the radial location at $r = 0$ does not correspond to the origin of the Schwarzschild spacetime but rather to the location of the event horizon.^{13,14}

The curvature singularity being at $R = 0$ also shows that the Schwarzschild representation is distinguished in so far as described in these coordinates, the gravitational field source can now indeed be considered a massive point particle located at the origin. In contrast, for coordinate systems with radial coordinates of the form, say, $R' = R + \beta$, where $\beta \in \mathbb{R}_{>0}$, the origin of the Schwarzschild radial coordinate R is smeared onto a sphere of finite, nonzero radius $R' = \beta$, rendering the source a 2-sphere. However, both source location representations, i.e., a point source at $R = 0$ and a source smeared onto a 2-sphere at $R' = \beta$, are equivalent in that they have the same center of mass, and therefore yield the same gravitational effects. In other words, the gravitational effects of a point source at $R = 0$ and a source smeared onto the sphere at $R' = \beta$ are indistinguishable.

¹² According to Birkhoff's theorem (see, e.g., [18]), the exterior Schwarzschild solution of the vacuum Einstein field equations is unique on the specified coordinate range. More precisely, the theorem states that any C^2 vacuum solution of the Einstein field equations that is spherically symmetric in an open set U is locally isometric to the (maximally extended) Schwarzschild solution in U . Hence, the exterior Schwarzschild solution may also be used to describe dynamical scenarios as long as spherical symmetry is conserved and the process under consideration does not give rise to violations of the vacuum Einstein field equations, that is, volume changes of the source have to be radially symmetrically decreasing in nature and not expand the source into the originally vacuum region.

¹³ The event horizon is a (trapping) null hypersurface for which observers stationed at rest at infinity find that there exists no infalling (physical) matter-energy distribution in the Universe that can ever, as a direct consequence of gravitational time dilation, traverse it. In addition, while closing in on the event horizon, those observers see matter-energy distributions undergo gravitational redshifts, eventually leading to a full dimming at the horizon. For comoving observers, on the other hand, infalling matter-energy distributions may cross the event horizon unidirectionally in finite eigentime into a region of spacetime in which an inexorable dragging towards the curvature singularity at $r = 0$ occurs. Framed mathematically more rigorously, the event horizon is the future boundary of the causal past of future null infinity $\partial J^-(\mathcal{I}^+) \cap \mathfrak{M}$ (see Remark IV.3 for a more detailed discussion).

¹⁴ The concurrence of the spherical polar coordinate singularity at $r = 0$ and the location of the event horizon is a consequence of Schwarzschild relating, by suitably arranging the two constants of integration of the vacuum Einstein field equations, the former, and thus the supposed location of his source, to the location of the singularity of the metrical coefficient f_1 (which he refers to as a point of discontinuity), for he requires his solution to satisfy the continuity condition 4. specified in Footnote 11.

B. Modern Account of the Exterior Schwarzschild Solution and Kruskal's Maximal Analytic Extension

From a more modern point of view, the exterior Schwarzschild solution \mathbf{g} is extended to the pair $(\mathfrak{M}, \mathbf{g})$, called the exterior Schwarzschild spacetime, which is a smooth, connected, globally hyperbolic and asymptotically flat Lorentzian 4-manifold homeomorphic to $\mathbb{R}^2 \times S^2$, where the metric \mathbf{g} defined in Equation (5) in Schwarzschild coordinates $(t, r, \vartheta, \phi) \in \mathbb{R} \times (2M, \infty) \times (0, \pi) \times [0, 2\pi)$ is a spherically symmetric and static 1-parameter family of exact Petrov type D solutions of the vacuum Einstein field equations $\text{Ric}(\mathbf{g}) = \mathbf{0}$.¹⁵ Extending this Lorentzian 4-manifold across $r = 2M$ up to the origin at $r = 0$, which in Schwarzschild coordinates is a singular extension with a coordinate singularity at $r = 2M$, the manifold now consists of two connected components: the exterior component $B_I = \{(t, r, \vartheta, \phi) \mid t \in \mathbb{R}, r \in (2M, \infty), \vartheta \in (0, \pi), \phi \in [0, 2\pi)\}$, which is the domain of outer communication, and the interior component $B_{II} = \{(t, r, \vartheta, \phi) \mid t \in \mathbb{R}, r \in (0, 2M), \vartheta \in (0, \pi), \phi \in [0, 2\pi)\}$, which is the (future) trapped region.¹⁶ Then, the Schwarzschild metric expressed in the Schwarzschild coordinate representation is defined for all $r \in \mathbb{R}_{>0} \setminus \{2M\}$, nonstatic in the interior region B_{II} , and features two types of singularities, viz., a curvature singularity at $r = 0$,¹⁷ and the above-mentioned coordinate singularity at $r = 2M$.

Remark II.4. *The Schwarzschild time coordinate t is a Cauchy temporal function in the exterior region B_I , i.e., $t: B_I \rightarrow \mathbb{R}$ is a smooth function with future-directed, timelike gradient $\nabla t = g^{\mu\nu}(\partial_\mu t)\partial_\nu = (1 - 2M/r)^{-1}\partial_t$ for which the level sets $t^{-1}(\cdot)$ are smooth, spacelike Cauchy hypersurfaces (see, e.g., [1]). Thus, it yields a foliation of this region by smooth, spacelike Cauchy hypersurfaces. Due to the irregular behavior of the Schwarzschild coordinates at $r = 2M$, the level sets of t do not, however, foliate $B_I \cup B_{II}$.*

As our later focus with regard to the construction procedure of Penrose diagrams is on the maximal analytic extension of the exterior Schwarzschild spacetime, the so-called Kruskal extension,¹⁸ which has the same geometric and topological characteristics as the above exterior Schwarzschild spacetime except for the metric not being globally static anymore, we here summarize the main result of Kruskal's original 1960 paper [21] on the topic. In this paper, Kruskal demonstrates that the then so-called Schwarzschild singularity of the exterior Schwarzschild solution occurring at $r = 2M$ is merely apparent, and therefore not a real singularity, by employing a “seemingly simpler and more explicit” choice of coordinates (as compared to the coordinates used in the works of Kasner [20], Lemaître [23], Einstein and Rosen [11], Robertson [36], Synge [40], Finkelstein [14], and Fronsdal [16]) in which the Schwarzschild singularity is removed and which gives rise to the maximal analytic extension of the original Schwarzschild solution.^{19,20}

More precisely, Kruskal starts with the exterior Schwarzschild solution (5) expressed in the usual Schwarzschild coordinates $(t, r, \vartheta, \phi) \in \mathbb{R} \times (2M, \infty) \times (0, \pi) \times [0, 2\pi)$, although with signature $(3, 1, 0)$, and seeks coordinates $(v, u, \vartheta, \phi) \in \mathbb{R} \times \mathbb{R}_{>0} \times (0, \pi) \times [0, 2\pi)$ in which the metric is still spherically symmetric but radial light rays have slopes $du/dv = \pm 1$ *everywhere*, so that the light cone structure at each event agrees with that of Minkowski spacetime.²¹ Because these two conditions immediately give rise to the metric ansatz

$$\mathbf{g} = f(r)^2 [-dv \otimes dv + du \otimes du] + r^2 \mathbf{g}_{S^2},$$

a direct comparison with Schwarzschild's metric representation, requiring that the function $f(r)$ is finite

¹⁵ Here and in the following, we use the more common symbol r for the Schwarzschild radial coordinate R .

¹⁶ In other words, B_I and B_{II} are two disjoint regions separated by a singular hypercylinder at $r = 2M$.

¹⁷ The well-known fact of the inevitability of impinging onto this particular curvature singularity after having crossed the event horizon can be directly traced back to its spacelike nature.

¹⁸ The Kruskal extension is also the maximal Cauchy development of the exterior Schwarzschild spacetime.

¹⁹ Other at that time very influential coordinate systems for the exterior Schwarzschild solution not mentioned by Kruskal are, e.g., the ones by Flamm [15], Gullstrand [17], Painlevé [30, 31], and Weyl [44].

²⁰ Around the same time, Szekeres published the article [41], in which he presents essentially the same coordinate system (except for a different scaling) to also show that the Schwarzschild singularity at $r = 2M$, which he calls a “Schwarzschild hypercylinder,” is merely an apparent singularity removable by a suitable change of coordinates. In this paper, he furthermore provided one of the first systematic, coordinate-independent definitions of singularities of pseudo-Riemannian manifolds.

²¹ For historical accuracy, we here employ Kruskal's original coordinate terminology, that is, instead of the well-established present-day designators T and X for the Kruskal time and radial coordinates, respectively, we adopt the notation v and u . It is, however, paramount that Kruskal's notation is not to be confused with the standard notation for the various Eddington–Finkelstein coordinates below.

and nonzero for $v = 0 = u$, results in the coordinate transformation

$$\mathfrak{T}: \begin{cases} \mathbb{R} \times (2M, \infty) \times (0, \pi) \times [0, 2\pi) \rightarrow \mathbb{R} \times \mathbb{R}_{>0} \times (0, \pi) \times [0, 2\pi) \\ (t, r, \vartheta, \phi) \mapsto (v, u, \vartheta', \phi') \end{cases}$$

with

$$v = \sqrt{\frac{r}{2M} - 1} e^{r/(4M)} \sinh\left(\frac{t}{4M}\right), \quad u = \sqrt{\frac{r}{2M} - 1} e^{r/(4M)} \cosh\left(\frac{t}{4M}\right), \quad \vartheta' = \vartheta, \quad \text{and} \quad \phi' = \phi$$

for $|v| < u$ on the one hand, and the so-called Kruskal representation of the exterior Schwarzschild solution

$$g = \frac{32M^3 e^{-r(v,u)/(2M)}}{r(v,u)} [-dv \otimes dv + du \otimes du] + r^2 g_{S^2} \quad (6)$$

on the other hand. Here, the function $r(v, u)$ is a solution of the transcendental algebraic equation

$$\left[\frac{r}{2M} - 1 \right] e^{r/(2M)} = u^2 - v^2, \quad (7)$$

namely $r(v, u) = W_0(e^{-1}[u^2 - v^2])$, with W_0 being the principal branch of the Lambert W function. The Kruskal representation (6), which is, strictly speaking, only valid for $r > 2M$, may, however, be smoothly analytically extended across $r = 2M$ without the Schwarzschild singularity occurring. Thus, it is regular for all $r \in \mathbb{R}_{>0}$.

Remark II.5. *Even though the metric is of the same form when $r < 2M$, the transformation from Schwarzschild coordinates to Kruskal coordinates then reads*

$$\mathfrak{T}: \begin{cases} \mathbb{R} \times (0, 2M) \times (0, \pi) \times [0, 2\pi) \rightarrow \mathbb{R} \times \mathbb{R}_{>0} \times (0, \pi) \times [0, 2\pi) \\ (t, r, \vartheta, \phi) \mapsto (v, u, \vartheta', \phi') \end{cases}$$

with

$$v = \sqrt{1 - \frac{r}{2M}} e^{r/(4M)} \sinh\left(\frac{t}{4M}\right), \quad u = \sqrt{1 - \frac{r}{2M}} e^{r/(4M)} \cosh\left(\frac{t}{4M}\right), \quad \vartheta' = \vartheta, \quad \text{and} \quad \phi' = \phi$$

for $|u| < v < \sqrt{1 + u^2}$. Accordingly, the function $r(v, u)$ is now determined by the secondary branch W_{-1} of the Lambert W function, viz., $r(v, u) = W_{-1}(e^{-1}[v^2 - u^2])$.

We point out that the Kruskal extension is comprised of two images of the region $\{(t, r, \vartheta, \phi) \mid t \in \mathbb{R}, r \in (2M, \infty), \vartheta \in (0, \pi), \phi \in [0, 2\pi)\}$ exterior to the Schwarzschild singularity,²² that is,

$$B_I = \{(v, u, \vartheta, \phi) \mid v \in \mathbb{R}, u \in \mathbb{R}_{>0}, \vartheta \in (0, \pi), \phi \in [0, 2\pi) \text{ and } |v| < u\}$$

$$B_{III} = \{(v, u, \vartheta, \phi) \mid v \in \mathbb{R}, u \in \mathbb{R}_{>0}, \vartheta \in (0, \pi), \phi \in [0, 2\pi) \text{ and } |v| < -u\},$$

and of two images of the interior region $\{(t, r, \vartheta, \phi) \mid t \in \mathbb{R}, r \in (0, 2M), \vartheta \in (0, \pi), \phi \in [0, 2\pi)\}$, namely

$$B_{II} = \{(v, u, \vartheta, \phi) \mid v \in \mathbb{R}, u \in \mathbb{R}_{>0}, \vartheta \in (0, \pi), \phi \in [0, 2\pi) \text{ and } |u| < v < \sqrt{1 + u^2}\}$$

$$B_{IV} = \{(v, u, \vartheta, \phi) \mid v \in \mathbb{R}, u \in \mathbb{R}_{>0}, \vartheta \in (0, \pi), \phi \in [0, 2\pi) \text{ and } -\sqrt{1 + u^2} < v < -|u|\},$$

where the regions B_{III} and B_{IV} are obtained by simultaneously applying the discrete reversal isometries $v \mapsto v' = -v$ and $u \mapsto u' = -u$.²³ This extension is the *maximal* coordinate-singularity-free extension of the exterior Schwarzschild solution, which Kruskal proves argumentatively via the global behavior of geodesics.²⁴

²² Hence, the Kruskal extension possesses two asymptotic ends.

²³ The particular restrictions on the values of the Kruskal coordinates v and u in these regions arise directly from the respective ranges of the radial coordinate r according to Equation (7).

²⁴ Kruskal remarks that in his analytic extension, geodesics either run into the “barrier” of intrinsic singularities at $r = 0$ or can be continued indefinitely with respect to their “natural length,” which may be interpreted as test particles either falling into the black hole or escaping to infinity. This result precludes the existence of an even larger singularity-free extension.

III. BASIC IDEA BEHIND PENROSE DIAGRAMS

Before we explicitly mathematically construct and then visualize the Penrose diagram of the maximal analytic extension of the exterior Schwarzschild spacetime, we present the idea underlying—and the general framework together with a precise mathematical definition for—Penrose diagrams.²⁵ For this purpose, we let (\mathfrak{M}, g) be a smooth, connected, and time-oriented Lorentzian 4-manifold. In order to obtain a faithful 2-dimensional representation of this 4-dimensional manifold that comprises the central information on the global causal structure and on possible infinities, so that any causal relations can be accurately depicted on a finite-sized diagram, one has to, in a first step, either suitably project out two of the four dimensions or just consider a 2-dimensional restriction of the spacetime. As different restrictions of one and the same spacetime may lead to different Penrose diagrams each containing only information for a particular slice (cf. Remark IV.7 for the example of the nonextreme Kerr spacetime), it may seem favorable to work with projections, for then, although different projections may also result in different Penrose diagrams, they give rise to representations in which every point accounts for the entire extracted 2-dimensional submanifold.²⁶ More precisely, the nature of these projections should be such that they map onto preferred 2-dimensional submanifolds that can account for the causal structure of the full 4-dimensional Lorentzian manifold, while at the same time they project out suitable 2-dimensional (preferably compact) submanifolds. And since this is not possible for spacetimes of all geometric and topological structures, one needs to identify families of spacetimes admitting projections that preserve in a sense the 4-dimensional conformal structure, i.e., null geodesics in the 2-dimensional representative submanifold have to correspond to a certain pivotal subset of null geodesics in the original Lorentzian 4-manifold.²⁷ The simplest example of one such family is given by the so-called warped product spacetimes that consist of a product space $\mathfrak{M} = \mathfrak{M}_L^{(2)} \times \mathfrak{M}_R^{(2)}$ endowed with a metric of the form

$$g = g_L^{(2)} \oplus (f g_R^{(2)}) \quad \text{for } f: \mathfrak{M}_L^{(2)} \rightarrow \mathbb{R}_{>0}, \quad (8)$$

where $(\mathfrak{M}_L^{(2)}, g_L^{(2)})$ and $(\mathfrak{M}_R^{(2)}, g_R^{(2)})$ are 2-dimensional Lorentzian and Riemannian manifolds, respectively [28, Chapter 7]. As this product structure allows for the natural identification

$$T(\mathfrak{M}_L^{(2)} \times \mathfrak{M}_R^{(2)}) = T\mathfrak{M}_L^{(2)} \oplus T\mathfrak{M}_R^{(2)},$$

one obtains the splitting

$$g(Y_L + Y_R, Z_L + Z_R) = g_L^{(2)}(Y_L, Z_L) + f g_R^{(2)}(Y_R, Z_R)$$

for $Y_k, Z_k \in \Gamma(T\mathfrak{M}_k^{(2)})$, $k \in \{L, R\}$, so any null geodesic in $(\mathfrak{M}_L^{(2)}, g_L^{(2)})$ is also a null geodesic in (\mathfrak{M}, g) .²⁸ The relevant causal relations between different points in (\mathfrak{M}, g) can thus be simply analyzed by means of $(\mathfrak{M}_L^{(2)}, g_L^{(2)})$.²⁹ Combining this with a globally regular conformal compactification,³⁰ which conformally maps the entire possibly infinite spacetime into a region of finite size with infinity on the boundary, brings about the advantage that one can encode and visualize the global geometry and causal structure, particularly the light cone structure and infinity, in a finite-sized 2-dimensional conformal diagrammatic representation, the so-called Penrose diagrams.

Remark III.1. *Since the Lorentzian manifold $(\mathfrak{M}_L^{(2)}, g_L^{(2)})$ is of dimension two, it is indeed conformally flat, i.e., it is conformally equivalent³¹ to a subset of Minkowski spacetime $\mathbb{R}^{1,1}$ with its particular topology and causal structure. Furthermore, if (\mathfrak{M}, g) is spherically symmetric, one finds that $\mathfrak{M}_L^{(2)} \cong \mathfrak{M}/\text{SO}(3)$ and $\mathfrak{M}_R^{(2)} \cong S^2$, that is, every point of the associated Penrose diagram corresponds to a 2-sphere.*

²⁵ Details on the background and the construction of Penrose diagrams can also be found in, e.g., [3–6, 37].

²⁶ For the special case of spherically symmetric spacetimes, there is, however, no practical difference between projections and restrictions.

²⁷ Although spacetime symmetries are particularly helpful in finding such projections, they are, similar to the conditions of asymptotic and conformal flatness, not necessary for the construction of Penrose diagrams.

²⁸ In the 2-dimensional Penrose diagrams of spherically symmetric spacetimes, the global 4-dimensional light cone structure is fully preserved along radial null geodesics.

²⁹ For more details on the causal structure of spacetimes see, e.g., [24, 25].

³⁰ This particular type of compactification is locally angle-preserving, however, it does not necessarily locally preserve distances. This makes the metric $g_L^{(2)}$ locally conformally equivalent to the actual metric g (cf. Footnote 31). Consequently, although scales may overall change, the local geometry remains invariant.

³¹ Two metrics g and g' are conformally equivalent iff $g' = \lambda g$ for $\lambda \in C^\infty(\mathfrak{M}, \mathbb{R}_{>0})$.

Remark III.2. Penrose diagrams may, a priori, be constructed for all kinds of spacetimes (or for particular subsets thereof) possessing the product structure given in Equation (8), ranging from simple vacuum spacetimes to spacetimes generated by nontrivial, dynamically evolving energy-momentum distributions. And although Penrose diagrams are by themselves not capable of directly visualizing the energy-momentum distribution inherent to any nonvacuum spacetime because their standard construction procedure is not based on more than the metric structure and certain coordinatizations of the underlying spacetimes (energy-momentum distributions and their possible spatio-temporal evolutions are usually incorporated into Penrose diagrams manually afterwards), they still reveal the energy-momentum distributions' influences on the causal structures of spacetimes in qualitative analyses.

According to the above description of the general requirements, construction, and characteristics of Penrose diagrams, we may define a Penrose diagram in a more rigorous way as follows.

Definition III.3. Let $(\mathfrak{M}_L^{(2)}, g_L^{(2)})$ be a smooth, connected, time-oriented Lorentzian 2-manifold, possibly with a boundary, and $\mathcal{U} \subset \mathfrak{M}_L^{(2)}$ an open subset. Furthermore, let $\Phi: \mathcal{U} \rightarrow \mathbb{R}^2$ be a diffeomorphism for which

(C1) the closure $\bar{\mathcal{U}} = \mathfrak{M}_L^{(2)}$.

(C2) there exists a compact subset $\mathcal{V} \subset \mathbb{R}^2$ such that the image $\Phi(\mathcal{U}) \subset \mathcal{V}$.

(C3) the metric takes the form $g_L^{(2)} = \lambda \eta^{(2)}$, where $\lambda \in C^\infty(\mathcal{U}, \mathbb{R}_{>0})$ and $\eta^{(2)}$ is the 2-dimensional Minkowski metric.

A Penrose diagram is the pair (Φ, \mathcal{U}) , where the image of $\Phi(\mathcal{U})$ is called the domain of the Penrose diagram with the boundary of the closure of the image of $\Phi(\mathcal{U})$ representing conformal infinity of $\mathfrak{M}_L^{(2)}$.

Here, Conditions (C1) and (C2) ensure that the Penrose diagram comprises the entirety of $\mathfrak{M}_L^{(2)}$ and that it is a finite representation of $\mathfrak{M}_L^{(2)}$, respectively, which allows, inter alia, for a proper study of conformal infinity. Condition (C3) causes $\Phi(\mathcal{U})$ to be a conformal isometry from $(\mathcal{U}, g_L^{(2)})$ into a bounded subset $(\mathcal{V}, \eta^{(2)}) \subset \mathbb{R}^{1,1}$ of (conformal) 2-dimensional Minkowski spacetime,³² which preserves the causal structure of $(\mathfrak{M}_L^{(2)}, g_L^{(2)})$ everywhere in $(\mathcal{V}, \eta^{(2)})$.

IV. CONSTRUCTION PROCEDURE OF THE PENROSE DIAGRAM OF THE MAXIMALLY ANALYTICALLY EXTENDED SCHWARZSCHILD SPACETIME

A. Coordinate Representation for the Penrose Diagram

Having outlined the basic idea and the general framework, we come back to the implementation of the construction method of Penrose diagrams demonstrated for the example of the maximally analytically extended Schwarzschild spacetime. For this purpose, we recall the usual derivation procedure of a compactified variant of Kruskal–Szekeres spacetime coordinates, which not just covers the maximal analytic extension but also constitutes a suitable basis for the corresponding Penrose diagram as it gives rise to a metric representation that is of the particular warped product structure specified in Equation (8) and satisfies Conditions (C1)–(C3) in Definition III.3. We also explain in detail the reasoning behind all the steps of the procedure.³³ Our starting point for the construction is the exterior Schwarzschild solution expressed in Schwarzschild coordinates (5). In this representation, Schwarzschild's metric is singular and causal-type-reversing³⁴ at the event horizon at $r = 2M$ so that every light cone approaching the event horizon from the outside closes up and eventually at the horizon degenerates,³⁵ whereas inside the horizon light cones tilt over such that all future-directed paths are, instead of the direction of increasing Schwarzschild time coordinate t as in the exterior, in the direction of decreasing Schwarzschild radial coordinate r . We thus require a single, globally well-defined coordinate representation of the

³² Throughout the paper, we denote Minkowski spacetime $(\mathbb{R}^n, \eta^{(n)})$ of total dimension n by $\mathbb{R}^{1,n-1}$.

³³ The steps involved are in essence a series of particular coordinate transformations.

³⁴ More precisely, this means that the gradient ∇t , associated with the Schwarzschild time coordinate t , which is timelike outside the event horizon, becomes spacelike inside the event horizon, and vice versa for the gradient ∇r that corresponds to the Schwarzschild radial coordinate r (see also Remark II.4).

³⁵ This can be easily seen from the fact that $dt/dr \rightarrow \pm\infty$ along outgoing and ingoing radial null geodesics approaching the event horizon at $r = 2M$, respectively, which gives rise to the aperture of the light cone tending to zero.

metric covering the entire maximal analytic extension. Such a representation is naturally regular at the event horizon, where the horizon is necessarily located at finite coordinate values and not shifted to infinity, and furthermore preserves the causal types of the coordinates throughout the extension. To determine a coordinate system that gives rise to the desired representation of the metric, we apply, in a first step, a transformation from the Schwarzschild coordinates into Eddington–Finkelstein double-null coordinates^{36,37}

$$\mathfrak{T}^{\text{EF}}: \begin{cases} \mathbb{R} \times \mathbb{R}_{>0} \setminus \{2M\} \times (0, \pi) \times [0, 2\pi) \rightarrow \mathbb{R} \times \mathbb{R} \times (0, \pi) \times [0, 2\pi) \\ (t, r, \vartheta, \phi) \mapsto (u, v, \vartheta', \phi') \end{cases}$$

with

$$\left\{ \begin{array}{ll} u = +t - r_\star & \text{and } v = +t + r_\star \quad \text{for } B_I \\ u = +t + r_\star & \text{and } v = -t + r_\star \quad \text{for } B_{II} \\ u = -t + r_\star & \text{and } v = -t - r_\star \quad \text{for } B_{III} \\ u = -t - r_\star & \text{and } v = +t - r_\star \quad \text{for } B_{IV} \end{array} \right\}, \quad \vartheta' = \vartheta, \quad \text{and} \quad \phi' = \phi, \quad {}^{38,39} \quad (9)$$

where

$$r_\star := r + 2M \ln \left| \frac{r}{2M} - 1 \right| \in \begin{cases} \mathbb{R} & \text{for } B_I \text{ and } B_{III} \\ \mathbb{R}_{<0} & \text{for } B_{II} \text{ and } B_{IV} \end{cases} \quad (10)$$

is the Regge–Wheeler coordinate, and $u < -v$ in B_{II} and $u > -v$ in B_{IV} . These coordinates are adapted to outgoing and ingoing radial null geodesics in the sense that the former geodesics satisfy the constraint $u = \text{const.}$, whereas for the latter the constraint $v = \text{const.}$ holds. Accordingly, if we decrease the Schwarzschild radial coordinate r along such a radial null curve with $u = \text{const.}$ ($v = \text{const.}$), we can now pass through the past (future) branch of the event horizon from region B_I into region B_{IV} (B_{II}) in a regular manner [cf. the dashed lines in FIG. 1(b)].⁴⁰ Nonetheless, the event horizon has now been pushed to infinity, viz., to $\{(u, v, \vartheta, \phi) \mid u \in \mathbb{R}, v = -\infty, \vartheta \in (0, \pi), \phi \in [0, 2\pi)\}$ in B_I and B_{II} , $\{(u, v, \vartheta, \phi) \mid u = \infty, v \in \mathbb{R}, \vartheta \in (0, \pi), \phi \in [0, 2\pi)\}$ in B_I and B_{IV} , $\{(u, v, \vartheta, \phi) \mid u = -\infty, v \in \mathbb{R}, \vartheta \in (0, \pi), \phi \in [0, 2\pi)\}$ in B_{II} and B_{III} , and $\{(u, v, \vartheta, \phi) \mid u \in \mathbb{R}, v = \infty, \vartheta \in (0, \pi), \phi \in [0, 2\pi)\}$ in B_{III} and B_{IV} . Furthermore, since the exterior Schwarzschild solution expressed in Eddington–Finkelstein double-null coordinates reads

$$\mathbf{g} = \frac{1}{2} \left| 1 - \frac{2M}{r(u, v)} \right| (du \otimes dv + dv \otimes du) - r(u, v)^2 \mathbf{g}_{S^2} \quad (11)$$

with the multivalued function⁴¹

$$r(u, v) = 2M \left[1 + \begin{cases} W_0(e^{\pm(v-u)/(4M)-1}) & \text{for } B_I/B_{III} \\ W_{-1}(-e^{\pm(v+u)/(4M)-1}) & \text{for } B_{II}/B_{IV} \end{cases} \right]$$

[cf. the solution to Equation (7) and Remark II.5], the metric determinant in this representation vanishes at $r = 2M$, rendering the exterior Schwarzschild solution not invertible at the event horizon and thus

³⁶ For a detailed discussion of the original Eddington–Finkelstein coordinates see Section V A 1. Their null variant, which we termed *Penrose coordinates*, are reviewed in Section V A 2.

³⁷ A coordinate v is called a null coordinate if the associated gradient ∇v satisfies the null condition $\mathbf{g}(\nabla v, \nabla v) = 0$.

³⁸ This particular set of four different region-wise transformation laws is required to obtain a consistent double-null coordinate covering of the maximal analytic extension $\bigcup_{i=I}^{IV} B_i$ of the exterior Schwarzschild solution that joins together the respective regions in an analytic manner, so that across overlapping edges the coordinate curves of $u(t, r_\star)$ and $v(t, r_\star)$ are carried over continuously while properly accounting for the multivaluedness of the Schwarzschild time coordinate t and of the Regge–Wheeler coordinate r_\star [see the orientations of the (u, v) and (t, r_\star) coordinate systems depicted in FIG. 1(b)].

³⁹ As in the case of Kruskal’s maximal analytic extension presented at the end of Section II A, the particular forms of the transformation laws for the Eddington–Finkelstein double-null coordinates u and v in the regions B_{III} and B_{IV} follow directly from applying the discrete reversal isometries $u \mapsto -u$ and $v \mapsto -v$ to the transformation laws for the regions B_I and B_{II} , respectively, which reverses the light cone structure in these regions.

⁴⁰ In Schwarzschild coordinates this was not possible for the Schwarzschild time coordinate along ingoing/outgoing radial null geodesics tends to $\pm\infty$ at the horizons.

⁴¹ Here, the upper signs in the exponential functions correspond to the regions denoted to the left of the forward slash in the attributions, while the lower signs pertain to the regions to the right of the forward slash. We continue using this particular notation in the remainder of the paper when necessary.

leaving it still degenerate.⁴² And although one may “traverse” the past and future event horizons by following outgoing and ingoing radial null geodesics for constant values of the coordinates u and v , respectively, these double-null coordinates, similar to the Schwarzschild coordinates (t, r) , only cover each of the four blocks of the maximal analytic extension separately, where they take values in all of \mathbb{R} [see again FIG. 1(b)]. Accordingly, they do not globally cover the unions $B_I \cup B_{II}$, $B_I \cup B_{IV}$, or $B_I \cup B_{II} \cup B_{IV}$, as do, e.g., advanced and retarded Eddington–Finkelstein coordinates (v, r) and (u, r) in the case of the first and second of these unions, respectively (for more details see Remark IV.1 below). Moreover, the Lorentzian component $\mathbf{g}_L^{(2)}$ [cf. Equation (8)] of the metric representation (11) is already conformally related to the 2-dimensional Minkowski metric $\boldsymbol{\eta}^{(2)} = (du \otimes dv + dv \otimes du)/2$ described in double-null coordinates $\mathbb{R} \times \mathbb{R} \ni (u, v) = (t - r, t + r)$.

Remark IV.1. *Choosing coordinates $(t, r_*, \vartheta, \phi) \in \mathbb{R} \times \mathbb{R} \times (0, \pi) \times [0, 2\pi)$ for which the representation of the exterior Schwarzschild metric becomes*

$$\mathbf{g} = \left(1 - \frac{2M}{r(r_*)}\right) (dt \otimes dt - dr_* \otimes dr_*) - r(r_*)^2 \mathbf{g}_{S^2},$$

where the multivalued function $r(r_*)$ is of the form

$$r(r_*) = 2M \left[1 + \begin{cases} W_0(e^{r_*/(2M)-1}) & \text{in the radial branch } r > 2M \text{ with } r_* \in \mathbb{R} \\ W_{-1}(-e^{r_*/(2M)-1}) & \text{in the radial branch } r < 2M \text{ with } r_* \in \mathbb{R}_{<0} \end{cases} \right],$$

we encounter the same problems as for the above Eddington–Finkelstein double null coordinates, i.e., even though at the event horizon at $r = 2M$ light cones do not close up anymore as a consequence of the change of radial coordinates⁴³ and none of the metric coefficients tend to infinity, the horizon has been pushed to $r_* = -\infty$ and the representation is not invertible. For advanced Eddington–Finkelstein spacetime coordinates $(v, r, \vartheta, \phi) \in \mathbb{R} \times \mathbb{R}_{>0} \times (0, \pi) \times [0, 2\pi)$, where $v = t + r_* - r$, however, the situation is different as the Schwarzschild time coordinate t is replaced with a new time coordinate v that changes constantly along ingoing radial null geodesics, so that progressions in this direction do not become slower and slower anymore.⁴⁴ In this case, in addition to the light cones still being well-behaved throughout the entire coordinate range,⁴⁵ the event horizon is obviously located at a finite coordinate value and, since the coordinate representation of the exterior Schwarzschild metric is given by

$$\mathbf{g} = \left(1 - \frac{2M}{r}\right) dv \otimes dv - \frac{2M}{r} (dv \otimes dr + dr \otimes dv) - \left(1 + \frac{2M}{r}\right) dr \otimes dr - r^2 \mathbf{g}_{S^2},$$

the metric determinant $\det(\mathbf{g}) = -r^4 \sin^2(\vartheta)$ does not vanish at $r = 2M$, thus showing the invertibility of the metric at the horizon. Yet, advanced Eddington–Finkelstein coordinates can only be analytically extended to cover the region $B_I \cup B_{II}$. They cannot be analytically extended in such a way that they cover the entire maximal analytic extension $\bigcup_{i=I}^{IV} B_i$.

⁴² In contrast, the determinant of the Schwarzschild representation of the exterior Schwarzschild solution is nonzero everywhere. However, in this case, this does not allow for any conclusions to be drawn about the invertibility at the event horizon at $r = 2M$, for it is not part of the coordinate range so that, strictly speaking, the determinant cannot be evaluated at the event horizon in the first place.

⁴³ Since now $dt/dr_* \rightarrow \pm 1$ along outgoing and ingoing radial null geodesics approaching the event horizon at $r = 2M$, respectively, the aperture of light cones expressed in these coordinates corresponds to the usual 45° aperture of light cones in Minkowski spacetime.

⁴⁴ The same holds for retarded Eddington–Finkelstein spacetime coordinates $(u, r, \vartheta, \phi) \in \mathbb{R} \times \mathbb{R}_{>0} \times (0, \pi) \times [0, 2\pi)$, with $u = t - r_* + r$, except that the time coordinate u changes constantly along *outgoing* radial null geodesics. For the advanced/retarded Eddington–Finkelstein null variants $(v/u, r, \vartheta, \phi) \in \mathbb{R} \times \mathbb{R}_{>0} \times (0, \pi) \times [0, 2\pi)$, where $v/u = t \pm r_*$ are null coordinates instead of time coordinates, there is no change at all, so that these null coordinates are even constant along ingoing/outgoing radial null geodesics.

⁴⁵ To be more precise, approaching the event horizon from the outside, the outgoing component of every light cone tilts over continuously until at the horizon it coincides with the horizon. On the inside, light cones never fully close up. As a consequence, all future-directed causal curves traversing the event horizon are trapped, eventually impinging on the curvature singularity. Besides, in contrast to the case of Schwarzschild coordinates where the time coordinate t and the radial coordinate r both change their causal type, now only the causal type of the Eddington–Finkelstein radial coordinate r reverses across the event horizon, i.e., the gradient ∇r transitions from being spacelike in the exterior region to being timelike in the interior region. The causal type of the Eddington–Finkelstein time coordinate v , on the other hand, is timelike in both the exterior and the interior region. The latter observation is consistent with v being a temporal function in $B_I \cup B_{II}$ (and similar for $B_{III} \cup B_{IV}$), which means that $v: B_I \cup B_{II} \rightarrow \mathbb{R}$ is a smooth function with future-directed, timelike gradient ∇v for which the level sets $v^{-1}(\cdot)$ are smooth, spacelike hypersurfaces (cf. Remark II.4 for the stronger notion of Cauchy temporal functions).

Next, in order to remove the inadequacies of the Eddington–Finkelstein double-null coordinates, we apply, in a second step, a transformation from these coordinates into compactified Kruskal–Szekeres double-null coordinates

$$\mathfrak{T}^{\text{KS1}}: \begin{cases} \mathbb{R} \times \mathbb{R} \times (0, \pi) \times [0, 2\pi) \rightarrow \left(-\frac{\pi}{2}, \frac{\pi}{2}\right) \times \left(-\frac{\pi}{2}, \frac{\pi}{2}\right) \times (0, \pi) \times [0, 2\pi) \\ (u, v, \vartheta, \phi) \mapsto (U, V, \vartheta', \phi') \end{cases}$$

with

$$\left\{ \begin{array}{lll} \tan(U) = -e^{-u/(4M)} & \text{and} & \tan(V) = +e^{v/(4M)} & \text{for } B_I \\ \tan(U) = +e^{u/(4M)} & \text{and} & \tan(V) = +e^{v/(4M)} & \text{for } B_{II} \\ \tan(U) = +e^{u/(4M)} & \text{and} & \tan(V) = -e^{-v/(4M)} & \text{for } B_{III} \\ \tan(U) = -e^{-u/(4M)} & \text{and} & \tan(V) = -e^{-v/(4M)} & \text{for } B_{IV} \end{array} \right\}, \quad \vartheta' = \vartheta, \quad \text{and} \quad \phi' = \phi, \quad (12)$$

where

$$\left\{ \begin{array}{lll} U \in (-\pi/2, 0) & \text{and} & V \in (0, \pi/2) & \text{for } B_I \\ U \in (0, \pi/2 - V) & \text{and} & V \in (0, \pi/2) & \text{for } B_{II} \\ U \in (0, \pi/2) & \text{and} & V \in (-\pi/2, 0) & \text{for } B_{III} \\ U \in (-\pi/2 - V, 0) & \text{and} & V \in (-\pi/2, 0) & \text{for } B_{IV} \end{array} \right\}.$$

These coordinates are globally well-defined with a single-valued, bounded range, i.e., they extend over—and cover in a regular manner—the entire maximal analytic extension $\bigcup_{i=I}^{IV} B_i$ of the exterior Schwarzschild solution compactified into a finite region.⁴⁶ Moreover, they locate the event horizon at finite coordinate values at $\{(U, V, \vartheta, \phi) \mid U = 0, V \in (-\pi/2, \pi/2), \vartheta \in (0, \pi), \phi \in [0, 2\pi)\}$ and $\{(U, V, \vartheta, \phi) \mid U \in (-\pi/2, \pi/2), V = 0, \vartheta \in (0, \pi), \phi \in [0, 2\pi)\}$ away from the boundary. In terms of compactified Kruskal–Szekeres double-null coordinates, the exterior Schwarzschild metric becomes

$$g = \frac{16M^3 e^{-r(U,V)/(2M)}}{\cos^2(U) \cos^2(V) r(U, V)} (dU \otimes dV + dV \otimes dU) - r(U, V)^2 g_{S^2},$$

in which $r(U, V)$ yields

$$r(U, V) = 2M [1 + W_{0/-1}(-e^{-1} \tan(U) \tan(V))] \quad \text{for } B_I \text{ and } B_{III}/B_{II} \text{ and } B_{IV}.$$

Represented in this form, the exterior Schwarzschild metric is regular over the entire maximal analytic extension with a globally nonvanishing determinant, so that it is invertible for all values $r \in \mathbb{R}_{>0}$ of the Schwarzschild radial coordinate.

Finally, for convenience and since spacetime coordinates are more customary than double-null coordinates, we transform the compactified Kruskal–Szekeres double-null coordinates into their spacetime variant.⁴⁷ To this end, we employ the transformation

$$\mathfrak{T}^{\text{KS2}}: \begin{cases} \left(-\frac{\pi}{2}, \frac{\pi}{2}\right) \times \left(-\frac{\pi}{2}, \frac{\pi}{2}\right) \times (0, \pi) \times [0, 2\pi) \rightarrow \left(-\frac{\pi}{4}, \frac{\pi}{4}\right) \times \left(-\frac{\pi}{2}, \frac{\pi}{2}\right) \times (0, \pi) \times [0, 2\pi) \\ (U, V, \vartheta, \phi) \mapsto (T, X, \vartheta', \phi') \end{cases}$$

with

$$T = \frac{U + V}{2}, \quad X = \frac{-U + V}{2}, \quad \vartheta' = \vartheta, \quad \text{and} \quad \phi' = \phi \quad \text{for } \bigcup_{i=I}^{IV} B_i, \quad (13)$$

⁴⁶ This particular compactification in terms of inverse tangent functions is merely chosen for simplicity and convenience. For there is, a priori, no preferred choice of squishing functions, there are naturally many other possibilities of invertible monotonic functions that map the given domains onto finite ranges.

⁴⁷ Expressing the Schwarzschild metric in terms of compactified Kruskal–Szekeres spacetime coordinates instead of compactified Kruskal–Szekeres double null coordinates not only makes the presence of the required metrical product structure for Penrose diagrams specified in Equation (8) more visible but also clearly shows that the Lorentzian component $g_L^{(2)}$ is a 2-dimensional conformally flat Minkowski metric.

TABLE I: Asymptotic relations between the Schwarzschild and Kruskal–Szekeres time and radial coordinates.

	$r \rightarrow \infty$	$r \rightarrow 2M$	$r \rightarrow 0$
B _I	$T = \pm[X - \pi/2], X \in [\pi/4, \pi/2]$	$T = \pm X, X \in [0, \pi/4]$	
B _{II}		$T = X , X \in [-\pi/4, \pi/4]$	$T = \pi/4, X \in (-\pi/4, \pi/4)$
B _{III}	$T = \pm[X + \pi/2], X \in [-\pi/2, -\pi/4]$	$T = \pm X, X \in [-\pi/4, 0]$	
B _{IV}		$T = - X , X \in [-\pi/4, \pi/4]$	$T = -\pi/4, X \in (-\pi/4, \pi/4)$
	$t \rightarrow \infty$	$t \rightarrow -\infty$	
B _I	$T = -[X - \pi/2], X \in [\pi/4, \pi/2]$	$T = [X - \pi/2], X \in [\pi/4, \pi/2]$	
	$T = X, X \in [0, \pi/4]$	$T = -X, X \in [0, \pi/4]$	
B _{II}	$T = -X, X \in [-\pi/4, 0]$	$T = X, X \in [0, \pi/4]$	
B _{III}	$T = -[X + \pi/2], X \in [-\pi/2, -\pi/4]$	$T = [X + \pi/2], X \in [-\pi/2, -\pi/4]$	
	$T = X, X \in [-\pi/4, 0]$	$T = -X, X \in [-\pi/4, 0]$	
B _{IV}	$T = -X, X \in [0, \pi/4]$	$T = X, X \in [-\pi/4, 0]$	

where

$$\left\{ \begin{array}{lll} T \in (|X - \pi/4| - \pi/4, -|X - \pi/4| + \pi/4) & \text{and} & X \in (0, \pi/2) & \text{for B}_I \\ T \in (|X|, \pi/4) & & X \in (-\pi/4, \pi/4) & \text{for B}_{II} \\ T \in (|X + \pi/4| - \pi/4, -|X + \pi/4| + \pi/4) & \text{and} & X \in (-\pi/2, 0) & \text{for B}_{III} \\ T \in (-\pi/4, -|X|) & & X \in (-\pi/4, \pi/4) & \text{for B}_{IV} \end{array} \right\}^{.48,49,50}$$

The exterior Schwarzschild metric represented in these coordinates reads

$$\mathbf{g} = \frac{32M^3 e^{-r(T,X)/(2M)}}{[\cos^2(T) - \sin^2(X)]^2 r(T,X)} (dT \otimes dT - dX \otimes dX) - r(T,X)^2 \mathbf{g}_{S^2},$$

with the multivalued function $r(T, X)$ also being determined by the principal and secondary branches of the Lambert W function,

$$r(T, X) = 2M \left[1 + \left\{ \begin{array}{ll} W_0(e^{-2 \operatorname{arccoth}(\cos(2T)/\cos(2X)) - 1}) & \text{for B}_I \text{ and B}_{III} \\ W_{-1}(-e^{-2 \operatorname{arctanh}(\cos(2T)/\cos(2X)) - 1}) & \text{for B}_{II} \text{ and B}_{IV} \end{array} \right\} \right].$$

⁴⁸ Geometrically, this transformation of the double-null coordinates U and V constitutes a simultaneous rotation of the U - V plane about 45° counterclockwise and scaling of the U and V axes by a factor of $1/\sqrt{2}$. Choosing a normalization constant of $1/\sqrt{2}$ instead of $1/2$ for the definition of the coordinates T and X would render the transformation a simple $SO(2)$ rotation of the above type but yield more cumbersome coordinate ranges.

⁴⁹ Expressed in terms of the Schwarzschild time coordinate t and the Regge–Wheeler coordinate r_* specified in Equation (10), the compactified Kruskal–Szekeres spacetime coordinates yield

$$T = \pm \frac{1}{2} \arctan \left(\frac{\sinh(t/(4M))}{\cosh(r_*/(4M))} \right) \quad \text{and} \quad X = \mp \frac{1}{2} \arctan \left(\frac{\cosh(t/(4M))}{\sinh(r_*/(4M))} \right) \pm \frac{\pi H(r_*)}{2} \quad \text{for B}_I/\text{B}_{III}$$

and

$$T = \mp \frac{1}{2} \arctan \left(\frac{\cosh(t/(4M))}{\sinh(r_*/(4M))} \right) \quad \text{and} \quad X = \mp \frac{1}{2} \arctan \left(\frac{\sinh(t/(4M))}{\cosh(r_*/(4M))} \right) \quad \text{for B}_{II}/\text{B}_{IV},$$

where $H(\cdot) := [1 + \operatorname{sgn}(\cdot)]/2$ is the usual Heaviside step function.

⁵⁰ Similar to the Schwarzschild time coordinate t in regions B_I and B_{III}, the Kruskal–Szekeres time coordinate T is a Cauchy temporal function in the maximal analytic extension $\bigcup_{i=1}^{\text{IV}} \text{B}_i$ of the exterior Schwarzschild solution.

B. Components of the Penrose Diagram

Now, to explicitly construct the Penrose diagram of the maximally analytically extended Schwarzschild spacetime, we have to identify the diagram's various components, viz., its boundary components and its interior regions, using the compactified Kruskal–Szekeres spacetime coordinates (13). To this end, it is convenient to employ the transcendental algebraic equations

$$\left\{ \begin{array}{l} \frac{\cos(2T)}{\cos(2X)} = -\coth(r_*(r)/(4M)) \quad \text{for } B_I \text{ and } B_{III} \\ \frac{\cos(2T)}{\cos(2X)} = -\tanh(r_*(r)/(4M)) \quad \text{for } B_{II} \text{ and } B_{IV} \end{array} \right\} \quad (14)$$

that relate the compactified Kruskal–Szekeres time and radial coordinates to the Regge–Wheeler coordinate and those relating the former to the Schwarzschild time coordinate

$$\left\{ \begin{array}{l} \frac{\sin(2T)}{\sin(2X)} = +\tanh(t/(4M)) \quad \text{for } B_I \text{ and } B_{III} \\ \frac{\sin(2T)}{\sin(2X)} = -\coth(t/(4M)) \quad \text{for } B_{II} \text{ and } B_{IV} \end{array} \right\},$$

from which one can directly read off the corresponding asymptotic relations presented in TABLE I.⁵¹ These asymptotics can then be employed to define the relevant exterior and interior boundary components of the Penrose diagram:

- (a) Future/past timelike infinity $i^\pm = (T = \pm\pi/4, X = \pi/4 \text{ in } B_I \text{ and } X = -\pi/4 \text{ in } B_{III})$.
- (b) Future/past null infinity $\mathcal{I}^\pm = \{(T, X) \mid T = \pm(-X + \pi/2) \text{ and } \pi/4 < X < \pi/2 \text{ in } B_I \text{ and } T = \pm(X + \pi/2) \text{ and } -\pi/2 < X < -\pi/4 \text{ in } B_{III}\}$.
- (c) Spacelike infinity $i^0 = (T = 0, X = \pm\pi/2)$.
- (d) The location of the curvature singularity at $\{(T, X) \mid T = \pm\pi/4 \text{ and } -\pi/4 < X < \pi/4\}$.
- (e) The event horizon $\mathfrak{H} = \mathfrak{H}^+ \cup \mathfrak{H}^-$ with $\mathfrak{H}^\pm = \{(T, X) \mid T = \pm X \text{ and } -\pi/4 \leq X \leq \pi/4\}$.

Accordingly, the total exterior boundary comprises conformal infinity and the curvature singularity, while the inner boundary consists of the future and past event horizon components \mathfrak{H}^\pm .

Remark IV.2. *The point $(T = 0, X = 0)$, the so-called bifurcation 2-sphere, is usually identified with a nontraversable wormhole, known as Einstein–Rosen bridge, connecting the two separated exterior regions B_I and B_{III} of the maximal analytic extension.*

Remark IV.3. *The exterior boundary component future null infinity \mathcal{I}^+ , which is a connected null curve with past limit point at spacelike infinity i^0 , can be used to give an adequate definition of the black hole region B_{II} , namely $\mathfrak{M} \setminus J^-(\mathcal{I}^+) \neq \emptyset$. Being the past boundary of this region, the future event horizon \mathfrak{H}^+ is thus canonically specified as $\partial J^-(\mathcal{I}^+) \cap \mathfrak{M}$. Interchanging the designators “future” and “past,” one may similarly define the white hole region B_{IV} and the past event horizon \mathfrak{H}^- .*

⁵¹ These equations can be directly derived via the transformations laws specified in Equations (9), (12), and (13) and basic trigonometric identities. More precisely, exemplified for the first transcendental algebraic equation given in Equation (14) for region B_I , this means that one begins by applying the transformation laws relating the Kruskal–Szekeres time and radial coordinates T and X to the Kruskal–Szekeres double-null coordinates U and V defined in Equation (13) to the quantity $\cos(2T)/\cos(2X)$, and then uses angle addition theorems, the Pythagorean trigonometric identity, and simple algebraic manipulations to obtain the expression

$$\frac{\cos(2T)}{\cos(2X)} = \frac{1 - \tan(U)\tan(V)}{1 + \tan(U)\tan(V)}. \quad (15)$$

Subsequently, inserting the transformation laws specified in Equation (9) for the region B_I into the corresponding transformation laws in Equation (12) and eliminating the functional dependence on the Schwarzschild time coordinate t , we find the relation

$$-\tan(U)\tan(V) = e^{r_*/(2M)} \quad (16)$$

between the Kruskal–Szekeres double-null coordinates U and V and the Regge–Wheeler coordinate r_* . Substituting Equation (16) into Equation (15) immediately yields the desired result. Besides, the particular forms of these transcendental algebraic equations were chosen for their simplicity and convenience in the evaluation of the asymptotic relations between the Schwarzschild and Kruskal–Szekeres time and radial coordinates shown in TABLE I.

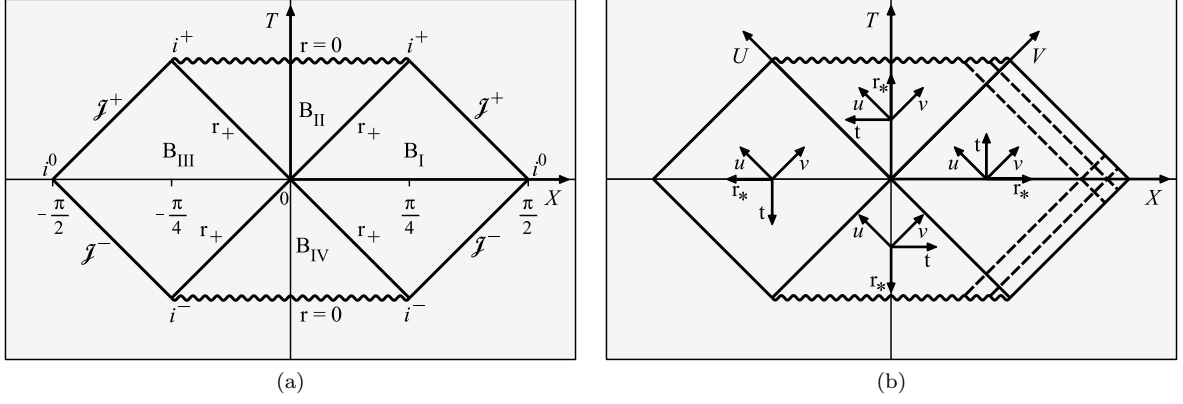


FIG. 1: (a) Penrose diagram of the Kruskal extension of the exterior Schwarzschild solution with labeling of the exterior and interior boundary structures and the different blocks, (b) the same diagram showing the orientations of the various coordinate systems paramount for its construction (scalings are suppressed for convenience) and displaying particular null hypersurfaces with $u = \text{const.}$ and $v = \text{const.}$ indicated by the dashed diagonal lines.

Moreover, the interior regions of the Penrose diagram, which are enclosed by the above boundary components, consist of the following four regions (cf. the end of Section II A):

$$\begin{aligned} B_I^{(2)} &= \{(T, X) \mid T \in (|X - \pi/4| - \pi/4, -|X - \pi/4| + \pi/4) \text{ and } X \in (0, \pi/2)\} \\ B_{II}^{(2)} &= \{(T, X) \mid T \in (|X|, \pi/4) \text{ and } X \in (-\pi/4, \pi/4)\} \\ B_{III}^{(2)} &= \{(T, X) \mid T \in (|X + \pi/4| - \pi/4, -|X + \pi/4| + \pi/4) \text{ and } X \in (-\pi/2, 0)\} \\ B_{IV}^{(2)} &= \{(T, X) \mid T \in (-\pi/4, -|X|) \text{ and } X \in (-\pi/4, \pi/4)\}. \end{aligned}$$

These four regions, in sequence, represent the exterior region,⁵² the interior black hole region, the parallel exterior region, and the interior white hole region, respectively.⁵³ Their composition together with the boundary components (a)–(e) make up the Penrose diagram of the entire maximally analytically extended Schwarzschild spacetime depicted in FIG. 1(a).

Remark IV.4. Although one might get the impression that in the Penrose diagram presented in FIG. 1(a) the curvature singularity at $r = 0$ is represented by curly spacelike curves that span either from future timelike infinity i^+ in B_I to its parallel counterpart in B_{III} or similarly for past timelike infinity i^- in B_I and B_{III} , these infinities are distinct from the curvature singularity, and thus from the two curly spacelike curves, for, e.g., in the case of the line between the future null infinities in B_I and B_{III} , every timelike curve in B_{II} reaches the curvature singularity even in finite coordinate time. Besides, all timelike curves in B_I that do not cross the event horizon never encounter the curvature singularity but eventually reach future timelike infinity. Besides, as can be directly seen from the orientation of the (t, r_*) coordinate system in B_{III} in FIG. 1(b), future/past timelike infinity i^\pm in this region of the Penrose diagram do not pertain to the “reversed” Schwarzschild time coordinate t but only to the compactified Kruskal–Szekeres time coordinate T .

Remark IV.5. Describing the Penrose diagram in FIG. 1(a) in terms of the original Schwarzschild coordinates $(t, r) \in \mathbb{R} \times \mathbb{R}_{>0} \setminus \{2M\}$, the compactified regions B_I and B_{III} of $\mathfrak{M}_L^{(2)}$ [see Equation (8)] each consist of a single connected set of points $\{(t, r) \mid t \in \mathbb{R} \text{ and } r \in (2M, \infty)\}$ for which the metric functions $g_{tt} = -1/g_{rr} = 1 - 2M/r$ of the Schwarzschild metric defined in Equation (5) are positive, whereas the compactified regions B_{II} and B_{IV} are each composed of the connected set $\{(t, r) \mid t \in \mathbb{R} \text{ and } r \in (0, 2M)\}$ with $g_{tt} = -1/g_{rr} = 1 - 2M/r$ being negative. Accordingly, each of these regions, which are nowadays frequently called “Boyer–Lindquist blocks,” is fully covered by the Schwarzschild metric (5) on the corresponding coordinate patch. However at their common boundary at $r = 2M$, which is a connected null hypersurface consisting of all points in $\mathfrak{M}_L^{(2)}$ for which $r = \text{const.}$

⁵² This region is also called the *domain of outer communication*.

⁵³ In the remainder of the paper, we drop the superscript “(2)” in the designators for these 2-dimensional regions for simplicity and convenience.

and $g_{tt} = 1/g_{rr} = 0$, the metric encounters a coordinate singularity. One may thus regard the union $\bigcup_{i=1}^{\text{IV}} B_i$ of the four compactified regions as a particular partition of $\mathfrak{M}_L^{(2)}$. Although in this partition there exists a one-to-one correspondence between the two radial intervals and the different types of blocks constituting $\mathfrak{M}_L^{(2)}$, the types being a full diamond and a half diamond, it contains two sets each of two blocks of the same type associated with the same radial interval, namely B_I and B_{III} for $(2M, \infty)$ and B_{II} and B_{IV} for $(0, 2M)$.

Remark IV.6. The construction procedure of the Penrose diagram of the maximal analytic extension of exterior Schwarzschild spacetime initially defined via the Schwarzschild representation (5), in which the 2-dimensional Lorentzian part of the metric $g_L^{(2)}$ reads

$$g_L^{(2)} = \left[1 - \frac{2M}{r}\right] dt \otimes dt - \left[1 - \frac{2M}{r}\right]^{-1} dr \otimes dr,$$

can be directly generalized to a construction procedure of Penrose diagrams of spacetimes with metrics possessing 2-dimensional Lorentzian parts of the form

$$g_L^{(2)} = \mathcal{F}(r) \mathcal{H}_1(r) dt \otimes dt - \mathcal{F}(r)^{-1} \mathcal{H}_2(r) dr \otimes dr, \quad (17)$$

where $\mathcal{F} \in C^\infty(\mathbb{R}, \mathbb{R})$ is analytic and $\mathcal{H}_{1/2} \in C^\infty(\mathbb{R}, \mathbb{R}_{>0})$.⁵⁴ The different steps in the construction procedure of these Penrose diagrams are identical to the ones for the Schwarzschild case, i.e., in order to bring the 2-dimensional metric specified in Equation (17) into the required manifestly conformally flat form, one first introduces the Regge–Wheeler coordinate

$$r_\star(r) = \int_c^r \widetilde{\mathcal{F}}(s)^{-1} ds, \quad (18)$$

where $\widetilde{\mathcal{F}} := \mathcal{F} \sqrt{\mathcal{H}_1/\mathcal{H}_2}$ and the value of the constant c has to be chosen such that $\widetilde{\mathcal{F}}(c) \neq 0$ [cf. Equation (10)]. For this purpose, one considers disjoint, maximal intervals in \mathbb{R} on which the function \mathcal{F} is both finite and does not change sign [as in the Schwarzschild case, where these maximal intervals are given by $(2M, \infty)$ and $(0, 2M)$]. This gives rise to connected Lorentzian 2-manifolds (the aforementioned, so-called blocks) on which $g_L^{(2)}$ is in general well-defined only separately, and which, if possible, are to be suitably patched together at their respective conjunctive null hypersurfaces (horizons) determined by $\widetilde{\mathcal{F}} = 0$, where the metric may exhibit a coordinate singularity.⁵⁵ Subsequently, one defines a set of double-null coordinates (u, v) with possibly infinite ranges on each block [cf. Equation (9)], which is finally transformed into a single regular double-null coordinate system (U, V) with finite ranges that covers the totality of all blocks [cf. Equation (12)].

Remark IV.7. Although particular spacetimes, such as the nonextreme Kerr spacetime (for details see, e.g., [3, 27]), which is the canonical rotating generalization of the Schwarzschild spacetime, do not possess the required product structure specified in Equation (8) (due to nonvanishing cross terms resulting from the presence of nonzero angular momentum generating rigid rotations around the symmetry axis), they nonetheless allow for the possibility of drawing Penrose diagrams for certain fixed values of the polar angular coordinate ϑ and/or the azimuthal angular coordinate ϕ , where, accordingly, the points in these Penrose diagram now do not correspond to “separated” 2-spheres as in the Schwarzschild case. [The standard Penrose diagram for the (maximally extended) nonextreme Kerr spacetime visualizes the geometry of the 2-dimensional submanifold along the symmetry axis for $\vartheta \in \{0, \pi\}$ and arbitrary values of ϕ [2]. Different Penrose diagrams of the nonextreme Kerr spacetime, such as the one for the equatorial plane at $\vartheta = \pi/2$, are discussed in, e.g., [4].] Consequently, this does not allow for inferences about the full 4-dimensional geometry to be drawn and globally useful information to be extracted as is the case for the Schwarzschild spacetime. For a 2-dimensional generalization of Penrose diagrams, the so-called projection diagrams, that does not suffer from this issue see also [4].

V. APPLICATION TO EDDINGTON–FINKELSTEIN AND PENROSE FOLIATIONS

In the following, we present the Penrose diagram of the maximally analytically extended Schwarzschild spacetime equipped with, on the one hand, a foliation by the level sets of the time coordinate of the

⁵⁴ For more details see [4].

⁵⁵ Although the particular value of the constant c in the Regge–Wheeler coordinate (18) could, a priori, be chosen differently in each of these blocks, a careful analysis shows it to be necessarily identical everywhere for ultimately one aims at constructing a single, globally regular double-null coordinate system covering the entire underlying spacetime.

canonical Eddington–Finkelstein representation and, on the other hand, a foliation by the level sets of the null coordinate of the Penrose representation. These visualizations allow us to easily work out the main properties of— and hence the differences between—these representations by direct inspection. To have the proper background, we first briefly recall the main results of the seminal research papers by Eddington, Finkelstein, and Penrose [8, 14, 35] pertaining to their coordinate representations of the exterior Schwarzschild solution.

A. Historical Remarks on the Eddington–Finkelstein and Penrose Representations of the Exterior Schwarzschild Solution

1. Eddington–Finkelstein Coordinates

We begin with the discovery of Eddington’s coordinates for the exterior Schwarzschild solution detailed in the 1924 paper [8], which was not, contrary to what one may expect, motivated by a resolution of the Schwarzschild singularity at $r = 2M$, and in that way uncovering that it is a mere coordinate singularity. It was rather a technical byproduct in a mathematical proof to demonstrate his claim of an exact equality of the Schwarzschild line element ds of Einstein’s general theory of relativity and the corresponding quantity dJ of Whitehead’s theory of gravitation [45], which both play an integral part in the determination of the paths taken by test particles in the gravitational field generated by a single massive point source.^{56,57}

More precisely, in his proof, Eddington considers the gravitational field of a massive point source at rest at the origin for which the line element expressed in Schwarzschild coordinates reads⁵⁸

$$ds^2 = \left[1 - \frac{2M}{r}\right] dt_1^2 - \left[1 - \frac{2M}{r}\right]^{-1} dr^2 - r^2(d\vartheta^2 + \sin^2(\vartheta) d\phi^2).$$

In order to bring this line element into the particular form of Whitehead’s expression for dJ^2 , he used the coordinate transformation from Schwarzschild coordinates to Whitehead’s coordinates

$$\mathfrak{T}: \begin{cases} \mathbb{R} \times (2M, \infty) \times (0, \pi) \times [0, 2\pi) \rightarrow \mathbb{R} \times (2M, \infty) \times (0, \pi) \times [0, 2\pi) \\ (t_1, r, \vartheta, \phi) \mapsto (t, r', \vartheta', \phi'), \end{cases}$$

with

$$t = t_1 - 2M \ln(r - 2M), \quad r' = r, \quad \vartheta' = \vartheta, \quad \text{and} \quad \phi' = \phi.⁵⁹$$

This coordinate transformation ensures that the outward speed of light in the radial direction is now unity everywhere, which is a paramount aspect of Whitehead’s theory. Moreover, it gives rise to the desired representation of the Schwarzschild line element

$$ds^2 = ds_{\mathbb{R}^{1,3}}^2 - \frac{2M}{r} (dt - dr)^2,$$

which is of the same form as dJ in Whitehead’s theory.^{60,61}

⁵⁶ To substantiate his equality assumption, Eddington points to the fact that the observed perihelion of Mercury and the observed deflection of light can be explained consistently within the frameworks of both theories, so “ dJ cannot be widely different from ds in the field of a single particle (the sun).”

⁵⁷ A strict equality between the expressions for ds and dJ , however, does not exist in the case of multiple gravitational-field-generating massive point particles. This is a consequence of the fact that in general relativity the overall gravitational effect of these point particles arises from a particular nonlinear coupling, whereas in Whitehead’s theory it is just a result of a simple superposition of the separate effects of the considered point particles.

⁵⁸ Instead of the usual symbol t , which Eddington reserves for Whitehead’s time coordinate, he denotes Schwarzschild’s time coordinate by $t_1 \in \mathbb{R}$.

⁵⁹ Eddington actually employs the time coordinate $t = t_1 - 2M \log(r - M)$, where $\log(\cdot)$ is regarded as the natural logarithm. Moreover, instead of $r - 2M$, the argument of the logarithm wrongly reads $r - M$ without the required prefactor of 2 in front of the second term.

⁶⁰ Here, $ds_{\mathbb{R}^{1,3}}^2$ is the line element in 4-dimensional Minkowski spacetime $\mathbb{R}^{1,3}$.

⁶¹ The associated metric in today’s well-known standard form is given by

$$g = \left[1 - \frac{2M}{r}\right] dt \otimes dt - \left[1 + \frac{2M}{r}\right] dr \otimes dr + \frac{2M}{r} (dt \otimes dr + dr \otimes dt) - r^2 g_{S^2}.$$

Remark V.1. *Eddington's coordinates are proper spacetime coordinates with a temporal function $t: B_I \rightarrow \mathbb{R}$ (cf. Footnote 45). Moreover, although they are only defined for the exterior region B_I , they can be analytically extended across the past event horizon to also cover region B_{IV} . The Schwarzschild metric in the corresponding Eddington representation is time-independent and regular at the event horizon at $r = 2M$ (with a nonsingular inverse).⁶²*

Next, we proceed with Finkelstein's seminal 1958 paper [14] on a potential past-future asymmetry of the gravitational field of a spherical point particle, where he constructs what he calls the *complete* analytic extension of the exterior Schwarzschild solution, which is considered to hold throughout all of the particle's (empty) spacetime and to possess no singularities⁶³ except for the one at the origin, that is, the location of the point particle itself. Based on this specific analytic extension, he intends to show that although the Einstein field equations allow for time inversions, i.e., they do not single out a preferred direction of time, there exist particular solutions to these equations, specifically the gravitational field of a spherical point particle, for which such a distinction—and thus a past-future asymmetry—naturally arises.⁶⁴

In more detail, Finkelstein models the spacetime (\mathfrak{M}, g) of an isolated point particle (or in his own words “a universe containing a point particle”) as the entirety of what he calls “4-space,” a 4-dimensional analytic manifold \mathfrak{M} coordinatized by $(x^\mu)_{\mu \in \{0,1,2,3\}}$, less the line $\mathcal{L} := \{(x^0, x^1, x^2, x^3) \mid x^0 \in \mathbb{R}, x^1 = x^2 = x^3 = 0\}$, i.e., the timeline of the point particle residing at the origin, and an analytic metric g satisfying the following eight physical conditions:

(C1) Solution of the vacuum Einstein field equations $R_{\mu\nu}(g) = 0$.

(C2) Invariant under the 1-parameter group of time translations

$$T_t: \begin{cases} x^0 \rightarrow \bar{x}^0 = x^0 - t \\ x^i \rightarrow \bar{x}^i = x^i. \end{cases}$$

(C3) Invariant under the connected 3-parameter group of spatial rotations

$$R_r: \begin{cases} x^0 \rightarrow \bar{x}^0 = x^0 \\ x^i \rightarrow \bar{x}^i = r_j^i x^j \end{cases}$$

with $r^T r = \mathbb{1}$ and $\det(r) = 1$.

(C4) Asymptotic to the Minkowski metric, i.e., $g_{\mu\nu} \rightarrow \eta_{\mu\nu}$ for $x^i x_i \rightarrow \infty$.⁶⁵

(C5) Not extendable to the line \mathcal{L} (excluding the trivial case $g_{\mu\nu} \equiv \eta_{\mu\nu}$).⁶⁶

(C6) Invariant under the discrete group of spatial reflections

$$P: \begin{cases} x^0 \rightarrow \bar{x}^0 = x^0 \\ x^i \rightarrow \bar{x}^i = -x^i. \end{cases}$$

(C7) Invariant under the discrete group of time inversions

$$T: \begin{cases} x^0 \rightarrow \bar{x}^0 = -x^0 \\ x^i \rightarrow \bar{x}^i = x^i. \end{cases}$$

(C8) The component $g_{00} > 0$ throughout \mathfrak{M} , so that x^0 is timelike.

⁶² The resolution of the Schwarzschild singularity is neither discussed nor even mentioned by Eddington in [8].

⁶³ Finkelstein employs the broader term “irregularities.”

⁶⁴ More precisely, the metric describing the spacetime of a massive, spherical point particle is not invariant under time reversal transformations $t \rightarrow \bar{t} = -t$ for any admissible choice of time coordinate.

⁶⁵ Finkelstein calls this metric the *Lorentz* metric.

⁶⁶ Finkelstein regards this line as a “true singularity.”

He goes on to show that for a point particle of *positive* mass, one already obtains a unique analytic metric

$$g = \left[1 - \frac{1}{r}\right] dx^0 \otimes dx^0 - \left[1 + \frac{1}{r}\right] dr \otimes dr + \frac{1}{r} (dx^0 \otimes dr + dr \otimes dx^0) - r^2 g_{S^2} \quad (19)$$

for coordinates $(x^0, r, \vartheta, \phi) \in \mathbb{R} \times (1, \infty) \times (0, \pi) \times [0, 2\pi)$ by imposing Conditions (C1)–(C5).^{67,68,69} This metric automatically satisfies Condition (C6), but it is incompatible with Conditions (C7) and (C8).⁷⁰ In particular, Finkelstein’s famous coordinate transformation for the exterior Schwarzschild solution enters the part of his proof where he establishes the validity of Condition (C1). More precisely, Finkelstein transforms the metric (19) into the usual Schwarzschild representation by using the coordinate transformation

$$\mathfrak{T}: \begin{cases} \mathbb{R} \times (1, \infty) \times (0, \pi) \times [0, 2\pi) \rightarrow \mathbb{R} \times (1, \infty) \times (0, \pi) \times [0, 2\pi) \\ (x^0, r, \vartheta, \phi) \mapsto (\bar{x}^0, \bar{r}, \vartheta', \phi') \end{cases}$$

with

$$\bar{x}^0 = x^0 + \ln(r - 1), \quad \bar{r} = r, \quad \vartheta' = \vartheta, \quad \text{and} \quad \phi' = \phi. \quad .^{71,72}$$

Then, since the Schwarzschild representation of the exterior Schwarzschild solution obviously satisfies $\bar{R}_{\mu\nu} = 0$ for $\bar{r} > 1$ and $R_{\mu\nu}$ is a tensor, he infers that also $R_{\mu\nu} = 0$ for $r > 1$. For $R_{\mu\nu}$ is analytic on \mathfrak{M} , he finally concludes that $R_{\mu\nu} = 0$ everywhere on \mathfrak{M} .

Remark V.2. *Since Finkelstein’s coordinates are, except for a normalization, in every respect identical to Eddington’s coordinates, they also have the properties established in Remark V.1. However, Finkelstein explicitly considers an analytic extension into the (nonstatic) domain for $r < 1$ (regularly across the past event horizon at $r = 1$), thus covering the region $B_I \cup B_{IV}$.⁷³*

Remark V.3. *Finkelstein deems the process of gravitational collapse of a star to be a transition from a manifold consisting of only the exterior region B_I to one of the manifolds of the two distinct but equivalent analytic extensions given by $B_I \cup B_{II}$ and $B_I \cup B_{IV}$, which both in his view represent the collapsed star. In this process, a singularity arises only at the origin at $r = 0$,⁷⁴ whereas the hypersurface at $r = 1$ is identified as a perfect unidirectional membrane, i.e., a hypersurface that can be crossed by causal influences only in one direction.⁷⁵*

Remark V.4. *Finkelstein argues for a past-future asymmetry⁷⁶ of the gravitational field of a spherical point particle on the basis of the corresponding (extended) spacetime being analytic and complete but featuring a metric that is not time-reversal invariant [cf. Equation (19)]. At the end of [14], however, he included a late footnote containing a “Note added in proof” that contradicts this view:*

Schild points out that \mathfrak{M} is still incomplete, it possesses a nonterminating geodesic of finite length in one direction. Kruskal has sketched for me a manifold \mathfrak{M}^ that is complete and contains \mathfrak{M} . \mathfrak{M}^* is time-symmetric and violates one of the conditions on \mathfrak{M} : it does not have the topological structure of all of 4-space less a line. Kruskal obtained \mathfrak{M}^* some years ago (unpublished).*

⁶⁷ Actually, Finkelstein employs an equivalent mixed Cartesian-spherical polar coordinate representation of the Schwarzschild metric.

⁶⁸ The Cartesian coordinates $(x^1, x^2, x^3) \in \mathbb{R}^3 \setminus \{0\}$ on which Finkelstein’s coordinates are, inter alia, based are all normalized to $2M$, resulting in a “mass-free” representation of the Schwarzschild metric.

⁶⁹ For the proof, Finkelstein defines the metric directly and then verifies the validity of Conditions (C1)–(C5). The uniqueness of a metric satisfying these conditions is taken as a well-known result. He does not, however, use the conditions to determine the metric in a constructive manner.

⁷⁰ For the details of Finkelstein’s reasoning see [14].

⁷¹ Finkelstein defines the transformation of the spatial coordinates more restrictively in terms of Cartesian coordinates.

⁷² This coordinate transformation gives rise to the *normalized* Schwarzschild representation

$$g = \left[1 - \frac{1}{\bar{r}}\right] d\bar{x}^0 \otimes d\bar{x}^0 - \left[1 - \frac{1}{\bar{r}}\right]^{-1} d\bar{r} \otimes d\bar{r} - \bar{r}^2 g_{S^2}.$$

⁷³ Finkelstein mentions the existence of another “distinct completion” of the exterior Schwarzschild solution simply obtained by time reversal. This analytic extension relates to a coordinate system that is now adapted to *ingoing* radial null geodesics with a time coordinate $\bar{x}^0 = x^0 - \ln|r - 1|$, covering the region $B_I \cup B_{II}$.

⁷⁴ The Schwarzschild singularity located at $r = 1$ was removed through Finkelstein’s coordinate transformation.

⁷⁵ The unidirectionality of the membranes of the two distinct analytic extensions is reversed.

⁷⁶ Finkelstein attributes this asymmetry to an “instability” caused by the nonlinearity of the theory.

This realization had to foil his conviction that time invariance and general relativity are incompatible for a spherical point source for Kruskal's result showed that the argumentation for a past-future asymmetry is based on the false premise of the completeness of the underlying manifold \mathfrak{M} , rendering the asymmetry to be merely an artifact ascribed to a too small choice of manifold. Kruskal's clarifying paper on the matter was eventually published in 1960 [21].

2. Penrose Coordinates

In his 1969 paper on the process of gravitational collapse in general relativity [35], which is in a sense a popularization of his famous 1965 singularity theorem paper [34], Penrose introduces and utilizes the transformation from Schwarzschild coordinates to coordinates featuring what he calls an advanced time parameter

$$\mathfrak{T}: \begin{cases} \mathbb{R} \times (2M, \infty) \times (0, \pi) \times [0, 2\pi) \rightarrow \mathbb{R} \times (2M, \infty) \times (0, \pi) \times [0, 2\pi) \\ (t, r, \vartheta, \phi) \mapsto (v, r', \vartheta', \phi') \end{cases}$$

with

$$v = t + r + 2M \ln(r - 2M), \quad r' = r, \quad \vartheta' = \vartheta, \quad \text{and} \quad \phi' = \phi,^{77} \quad (20)$$

for he aims at constructing an analytic extension of the exterior Schwarzschild solution across the future event horizon as a simple vacuum model of the deep interior region of a contracting star needed for the full description of the gravitational collapse process.

Remark V.5. Unlike Eddington's and Finkelstein's original spacetime coordinates, which feature besides three spatial coordinates a time coordinate that is a proper temporal function (cf. Section VA 1), Penrose's coordinates, although seemingly similar [but corresponding to Finkelstein's ingoing (or "time-reversed") coordinates and with an additional linear contribution $+r$], are null coordinates, i.e., in addition to the three spatial coordinates they are endowed with a null coordinate v instead of a time coordinate. The fact that v is a null coordinate in the first place can be traced back to it being in a sense adapted to the ingoing radial null geodesics in the exterior Schwarzschild spacetime. More precisely, this coordinate is fully derivable from the tangent vectors to these ingoing radial null geodesics (here defined in terms of Schwarzschild's coordinates)

$$\frac{dt_1}{ds} = \frac{r^2}{\Delta} \mathcal{E}_0 \quad \text{and} \quad \frac{dr}{ds} = -\mathcal{E}_0,$$

where s is an affine parameter and $\mathcal{E}_0 \in \mathbb{R}_{>0}$ a constant. Elimination of the affine parameter gives rise to the relation

$$\frac{dt_1}{dr} = -\left[1 - \frac{2M}{r}\right]^{-1} \Leftrightarrow t_1 = -r - 2M \ln\left|\frac{r}{2M} - 1\right| + C_0$$

between the time and radial coordinates, with $C_0 \in \mathbb{R}$ being a constant, which may be viewed as the basis underlying Penrose's coordinate transformation (20).

Remark V.6. Strictly speaking, Penrose's coordinates only account for the region B_I , which may be seen from the logarithmic contribution in the null coordinate v defined in Equation (20) in combination with the original range of the Schwarzschild radial coordinate $\text{Ran}(r) = (2M, \infty)$. However, they can be easily analytically extended across the future event horizon to also cover region B_{II} , where v has to be of the particular form

$$v = -t + r + 2M \ln(2M - r).$$

In terms of Penrose's coordinates, the exterior Schwarzschild solution takes the form

$$\mathbf{g} = \left[1 - \frac{2M}{r}\right] dv \otimes dv - dv \otimes dr - dr \otimes dv - r^2 \mathbf{g}_{S^2}.$$

⁷⁷ Penrose actually writes down the decadic logarithm $\log(\cdot)$ but treats it like the natural logarithm $\ln(\cdot)$ throughout his paper.

This representation, if properly analytically extended across the future event horizon into the nonstatic interior, is regular for all $r \in \mathbb{R}_{>0}$ (with a nonsingular inverse similar to the Eddington–Finkelstein case).⁷⁸

B. Comparison of Eddington–Finkelstein and Penrose Foliations

To bring out the differences between the Eddington–Finkelstein and Penrose coordinate representations of the exterior Schwarzschild solution, which we have already briefly addressed in Remark V.5, we visually analyze—and then contrast—Penrose diagrams of the maximal analytic extension of the exterior Schwarzschild solution with the region $B_I \cup B_{II}$ foliated by the level sets of Eddington’s and Finkelstein’s time coordinate v_{EF} on the one hand, and Penrose’s null coordinate v_{Pen} on the other hand. This has the advantage that the differences can be directly read out without resorting to any mathematical formalisms.

Remark V.7. *In order to directly compare these two coordinate representations, we have to consider the advanced form of the former coordinates, i.e., instead of using the retarded time coordinate $v_{\text{EF}} = t_S - \ln(r - 1)$, which is adapted to outgoing radial null geodesics, we work with the coordinate $v_{\text{EF}} = t_S + \ln(r - 1)$ being adapted to ingoing radial null geodesics.*⁷⁹

We begin with the Penrose diagram depicting the family of level sets of the advanced Eddington–Finkelstein time coordinate v_{EF} presented in FIG. 2(a). These level sets are all spacelike (at every point their slopes have an opening angle with the abscissa smaller than 45°) and extend from spacelike infinity i^0 to the curvature singularity $r = 0$, where they terminate. They cross smoothly from the exterior region B_I through the event horizon at $r = 2M$ into the black hole interior region B_{II} , preserving their spatio-temporal characteristics. In contrast, FIG. 2(b) shows the Penrose diagram with the family of level sets of the Penrose null coordinate $v_{\text{Pen}} = t_{\text{EF}} + r$, which are all null hypersurfaces (with 45° -angled slopes with respect to the abscissa at every point) beginning at past null infinity \mathcal{I}^- , traverse the event horizon smoothly while maintaining their null characteristics, and also terminating at $r = 0$. In a nutshell, the differences between Eddington’s and Finkelstein’s coordinates introduced in [8, 14] and Penrose’s coordinates employed in [35] essentially amount to the former coordinates being the retarded type of the spacetime variant, whereas the latter coordinates are the advanced type of the null variant (with the Eddington–Finkelstein time coordinate v_{EF} being a proper temporal function and the Penrose time coordinate v_{Pen} a null coordinate).

Remark V.8. *For the construction of the family of level sets of, e.g., the advanced Eddington–Finkelstein time coordinate v_{EF} in the region $B_I \cup B_{II}$, one first derives an algebraic equation relating the Kruskal–Szekeres time and radial coordinates T and X to the advanced Eddington–Finkelstein time coordinate v_{EF} . To this end, one substitutes the global transformation laws $U = T - X$ and $V = T + X$ for the Kruskal–Szekeres double-null coordinates U and V [cf. Equation (13)] and the transformation laws for the Eddington–Finkelstein double-null coordinates u and v in the regions B_I and B_{II} , which are specified in Equation (9), into Equation (12). Then, using the transformation laws $v_{\text{EF}} = t + r_*(r) - r$ and $r' = r$ between the advanced Eddington–Finkelstein time and radial coordinates v_{EF} and r' and the Schwarzschild time and radial coordinates t and r , one obtains the expressions*

$$\left\{ \begin{array}{l} \tan(T \pm X) = e^{(v_{\text{EF}} + r')/(4M)} \\ \tan(T \mp X) = \mp e^{-(v_{\text{EF}} - 2r_*(r') + r')/(4M)} \end{array} \right\} \quad \text{for } B_I/B_{II} \quad (21)$$

relating the Kruskal–Szekeres time and radial coordinates T and X and the advanced Eddington–Finkelstein time and radial coordinates v_{EF} and r' . Eliminating the advanced Eddington–Finkelstein time coordinate v_{EF} by multiplying the first and second sets of equations in Equation (21), and subsequently solving for the advanced Eddington–Finkelstein radial coordinate r' results in

$$r'(T, X) = 2M[1 + W_{0/-1}(-e^{-1} \tan(T + X) \tan(T - X))] \quad \text{for } B_I/B_{II}.$$

⁷⁸ Although Penrose did not work out the full coordinate transformation for the analytic extension across the future event horizon, he nonetheless points out that the Schwarzschild metric in this representation properly describes both regions B_I and B_{II} .

⁷⁹ More precisely, to properly cover the analytic extension $B_I \cup B_{II}$, we work with the advanced Eddington–Finkelstein time coordinate $v_{\text{EF}} = t_S + \ln|r - 1|$.

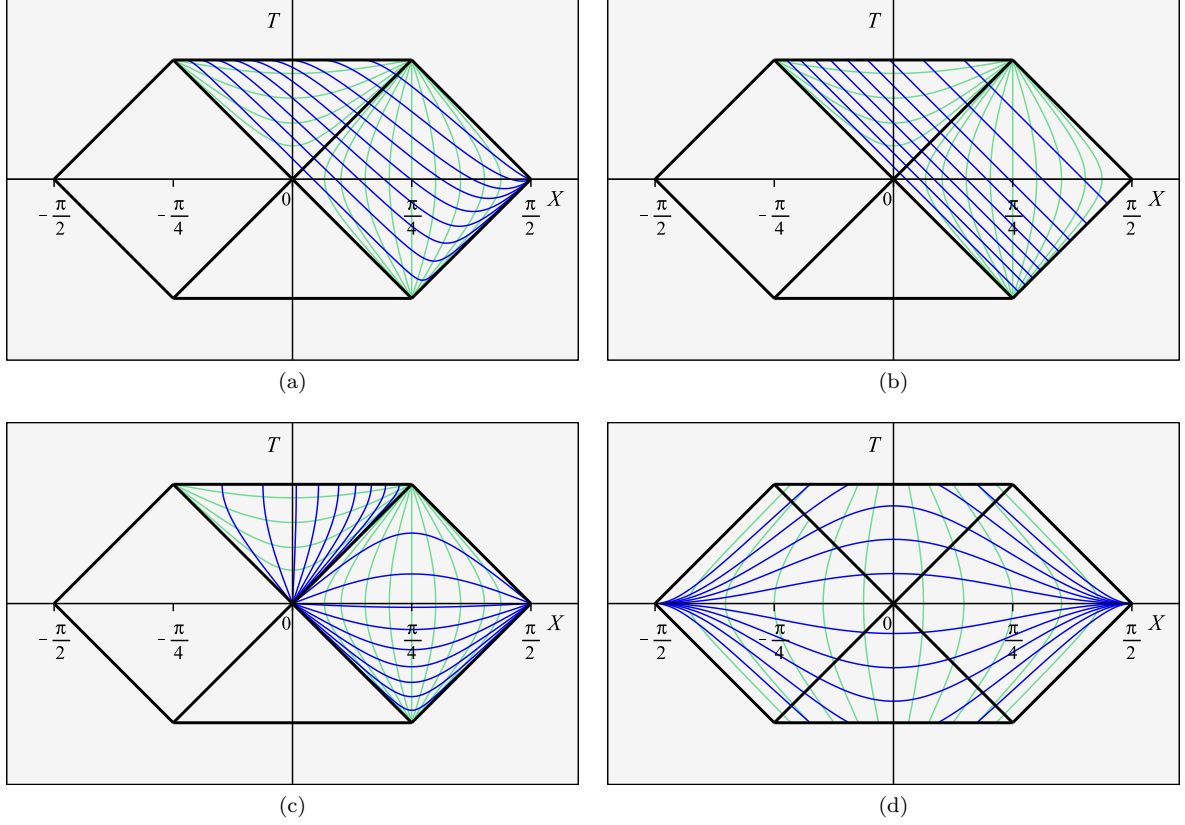


FIG. 2: (a) Penrose diagram of the Kruskal extension of the exterior Schwarzschild spacetime with level sets of the advanced Eddington–Finkelstein time coordinate v_{EF} (blue curves) and hypersurfaces of constant advanced Eddington–Finkelstein radius r (aquamarine curves). (b)–(d) the same diagram for the Penrose representation, the Schwarzschild representation extended to the region $B_I \cup B_{\text{II}}$, and the Kruskal–Szekeres representation, respectively.

Inserting this expression into Equation (21) and applying a series of simple algebraic manipulations yields the desired relation

$$2 \ln(\tan(T \pm X)) + e^{v_{\text{EF}}/(2M)} \tan(T \mp X) \cot(T \pm X) = \frac{v_{\text{EF}}}{2M} + 1 \quad \text{for } B_I/B_{\text{II}}.$$

The family of level sets of the advanced Eddington–Finkelstein time coordinate v_{EF} are now given by the solutions $\{T_{v_0}(X) \mid X \in (-\pi/4, \pi/2) \text{ and } v_{\text{EF}} = v_0 \in \mathbb{R}\}$ of these transcendental algebraic equations, where each constant v_0 uniquely determines one particular level set.

For completeness, we also discuss the Penrose diagrams containing foliations by spacelike and timelike hypersurfaces associated with the Schwarzschild and Kruskal–Szekeres time and radial coordinates depicted in FIG. 2(c) and FIG. 2(d), respectively (for the definitions of both coordinate systems see Sections II A and II B). In the former case, both hypersurfaces of constant Schwarzschild time t and hypersurfaces of constant Schwarzschild radius r are fully contained either in the exterior black hole region B_I or in the interior black hole region B_{II} , never crossing through—but asymptotically touching—the event horizon at $r = 2M$ that separates B_I from B_{II} .^{80,81} However, their causal types reverse across the event horizon, i.e., the spacelike hypersurfaces of constant Schwarzschild time in B_I (blue curves extending from spacelike infinity i^0 to the bifurcation 2-sphere at $(T = 0, X = 0)$ with slopes at every

⁸⁰ These hypersurfaces can also be drawn in the exterior region B_{III} and the interior region B_{IV} for the Schwarzschild coordinate system may be used to also cover these regions individually (the same holds for the Eddington–Finkelstein and Penrose cases for the region $B_{\text{III}} \cup B_{\text{IV}}$).

⁸¹ The (future) event horizon delineating B_I from B_{II} coincides with the level set of the Schwarzschild time coordinate tending to $+\infty$, which reflects the fact that an infalling test particle described in Schwarzschild coordinates takes an infinite coordinate time interval to reach the horizon. For Eddington–Finkelstein and Penrose coordinates, this time interval is finite.

point having an opening angle with the abscissa smaller than 45°) become timelike in B_{II} (blue curves extending from the bifurcation 2-sphere to the curvature singularity at $r = 0$ with slopes at every point having an opening angle with the abscissa larger than 45°) and vice versa for the timelike hypersurfaces of constant Schwarzschild radius [aquamarine curves extending from past timelike infinity i^- to future timelike infinity i^+ in B_I and extending from $(t = -\infty, r = 0)$ to $(t = +\infty, r = 0)$ in B_{II}]. Moreover, the shapes of the curves associated with hypersurfaces of constant Schwarzschild time depicted in the Penrose diagram look like parabolas in B_I , hyperbolas in B_{II} , and vice versa for the shapes of the curves associated with the hypersurfaces of constant Schwarzschild radius, with every family of curves bounded by a pair of event horizons at a 45° angle.

Finally, in the latter case of Kruskal–Szekeres coordinates that cover the maximal analytic extension, the spacelike hypersurfaces of constant Kruskal–Szekeres time v (blue curves with slopes at every point having an opening angle with the abscissa smaller than 45°) begin at spatial infinity i^0 in B_I , then cross into and traversing smoothly either B_{II} or B_{IV} , and end at spatial infinity i^0 in B_{III} . However, there also exist *separate*, mirror-symmetrical pairs of spacelike hypersurfaces for the same constant Kruskal–Szekeres time that originate at i^0 in B_I and i^0 in B_{III} , respectively, but terminate at the curvature singularity at $\{(T, X) | T = \pi/4 \text{ and } -\pi/4 \leq X \leq \pi/4\}$ without ever connecting along the line $\{(T, X) | X = 0\}$, thus generating a “forbidden range” in X . This particular progression can be explained by the constraint $v^2 < 1 + u^2$ for B_{II} and B_{IV} being violated for specific values of u if the Kruskal–Szekeres time coordinate v is, a priori, fixed exceeding a certain critical value.⁸² The timelike hypersurfaces of constant Kruskal–Szekeres coordinate u (aquamarine curves with slopes at every point having an opening angle with the abscissa larger than 45°) all start in B_{IV} at the past curvature singularity at $\{(T, X) | T = -\pi/4 \text{ and } -\pi/4 \leq X \leq \pi/4\}$ and end in B_{II} at the future curvature singularity at $\{(T, X) | T = \pi/4 \text{ and } -\pi/4 \leq X \leq \pi/4\}$, while in between smoothly passing through the region B_I or B_{III} , always preserving their causal types as do the spacelike hypersurfaces of constant Kruskal–Szekeres time.

Acknowledgments

The author is grateful to Dennis Lehmkuhl for suggesting to write a pedagogical paper on the construction and use of Penrose diagrams, and to work out the differences between the two different variants of Eddington–Finkelstein coordinates. He is also grateful to the Lichtenberg Group for History and Philosophy of Physics of the University of Bonn for useful discussions on the topic, and for detailed comments on the first draft of this paper. This project has received funding from the European Research Council (ERC) under the European Union’s Horizon 2020 research and innovation programme (grant agreement n°101088528, COGY) and from the Lichtenberg Grant for Philosophy and History of Physics of the Volkswagen Foundation.

-
- [1] A.N. Bernal and M. Sánchez, “Smoothness of time functions and the metric splitting of globally hyperbolic spacetimes,” *Communications in Mathematical Physics* **257**, pp. 43–50 (2005).
 - [2] B. Carter, “Complete analytic extension of the symmetry axis of Kerr’s solution of Einstein’s equations,” *Physical Review* **141**, pp. 1242–1247 (1966).
 - [3] S. Chandrasekhar, *The Mathematical Theory of Black Holes*, New York: Oxford University Press, 1983.
 - [4] P.T. Chruściel, C.R. Öz, and S.J. Szybka, “Space-time diagrammatics,” *Physical Review D* **86**, id. 124041 (2012).
 - [5] M. Dafermos and I. Rodnianski, “A proof of Price’s law for the collapse of a self-gravitating scalar field,” *Inventiones mathematicae* **162**, pp. 381–457 (2005).
 - [6] M. Dafermos and I. Rodnianski, “Lectures on black holes and linear waves,” *Clay Mathematics Proceedings* **17**, pp. 97–205 (2013).
 - [7] J. Droste, “The field of a single centre in Einstein’s theory of gravitation, and the motion of a particle in that field,” *Koninklijke Nederlandsche Akademie van Wetenschappen Proceedings* **19**, pp. 197–215 (1917).
 - [8] A.S. Eddington, “A comparison of Whitehead’s and Einstein’s formulae,” *Nature* **113**, p. 192 (1924).
 - [9] A. Einstein, “Erklärung der Perihelbewegung des Merkur aus der allgemeinen Relativitätstheorie,” *Sitzungsberichte der Königlich Preussischen Akademie der Wissenschaften zu Berlin*, pp. 831–839 (1915).

⁸² Cf. the constraints on the Kruskal–Szekeres coordinates v and u given in the definitions of the four regions B_I – B_{IV} of the maximal analytic extension at the end of Section II A.

- [10] A. Einstein, “Die Feldgleichungen der Gravitation,” *Sitzungsberichte der Königlich Preussischen Akademie der Wissenschaften zu Berlin*, pp. 844–847 (1915).
- [11] A. Einstein and N. Rosen, “The particle problem in the general theory of relativity,” *Physical Review* **48**, pp. 73–77 (1935).
- [12] J. Eisenstaedt, “The early interpretation of the Schwarzschild solution,” in: D. Howard and J. Stachel, *Einstein and the History of General Relativity*, Boston: Birkhäuser, 1989.
- [13] J. Eisenstaedt, “Lemaître and the Schwarzschild solution,” in: J. Earman, M. Janssen, and J.D. Norton, *The Attraction of Gravitation: New Studies in the History of General Relativity*, Boston: Birkhäuser, 1993.
- [14] D. Finkelstein, “Past-future asymmetry of the gravitational field of a point particle,” *Physical Review* **110**, pp. 965–967 (1958).
- [15] L. Flamm, “Beiträge zur Einsteinschen Gravitationstheorie,” *Physikalische Zeitschrift* **17**, pp. 448–454 (1916).
- [16] C. Fronsdal, “Completion and embedding of the Schwarzschild solution,” *Physical Review* **116**, pp. 778–781 (1959).
- [17] A. Gullstrand, “Allgemeine Lösung des statischen Einkörperproblems in der Einsteinschen Gravitationstheorie,” *Arkiv för Matematik, Astronomi och Fysik* **16**, pp. 1–15 (1921).
- [18] S.W. Hawking and G.F.R. Ellis, *The Large Scale Structure of Space-time*, New York: Cambridge University Press, 1973.
- [19] C. Heinicke and F.W. Hehl, “Schwarzschild and Kerr solutions of Einstein’s field equation: an introduction,” *International Journal of Modern Physics D* **24**, id. 1530006 (2015).
- [20] E. Kasner, “Finite representation of the solar gravitational field in flat space of six dimensions,” *American Journal of Mathematics* **43**, pp. 130–133 (1921).
- [21] M.D. Kruskal, “Maximal extension of Schwarzschild metric,” *Physical Review* **119**, pp. 1743–1745 (1960).
- [22] J.M. Lee, *Introduction to Smooth Manifolds*, New York: Springer, 2012.
- [23] G. Lemaître, “L’Univers en expansion,” *Annales de la Société Scientifique de Bruxelles A* **53**, pp. 51–85 (1933).
- [24] E. Minguzzi, “Lorentzian causality theory,” *Living Reviews in Relativity* **22**, 3 (2019).
- [25] E. Minguzzi and M. Sánchez, “The causal hierarchy of spacetimes,” in: H. Baum and D. Alekseevsky, *Recent Developments in Pseudo-Riemannian Geometry, ESI Lectures in Mathematics and Physics*, Zurich: European Mathematical Society Press, pp. 299–358, 2008.
- [26] C.W. Misner, K.S. Thorne, and J.A. Wheeler, *Gravitation*, San Francisco: W.H. Freeman and Company, 1973.
- [27] B. O’Neill, *The Geometry of Kerr Black Holes*, Wellesley: A K Peters, 1995.
- [28] B. O’Neill, *Semi-Riemannian Geometry with Applications to Relativity*, San Diego: Academic Press, 1983.
- [29] B. O’Neill, *Elementary Differential Geometry*, San Diego: Academic Press, 2006.
- [30] P. Painlevé, “La mécanique classique et la théorie de la relativité,” *Comptes Rendus de l’Académie des Sciences* **173**, pp. 677–680 (1921).
- [31] P. Painlevé, “La gravitation dans la mécanique de Newton et dans la mécanique d’Einstein,” *Comptes Rendus de l’Académie des Sciences* **173**, pp. 873–887 (1921).
- [32] R. Penrose, “Asymptotic properties of fields and space-times,” *Physical Review Letters* **10**, pp. 66–68 (1963).
- [33] R. Penrose, “Conformal treatment of infinity,” in: B. deWitt and C. deWitt, *Relativity, Groups and Topology*, New York, London: Gordon and Breach, pp. 565–584, 1964.
- [34] R. Penrose, “Gravitational collapse and space-time singularities,” *Physical Review Letters* **14**, pp. 57–59 (1965).
- [35] R. Penrose, “Gravitational collapse: the role of general relativity,” *Rivista del Nuovo Cimento* **1**, pp. 252–276 (1969).
- [36] H.P. Robertson and T.W. Noonan, *Relativity and Cosmology*, Philadelphia: W.B. Saunders, 1968.
- [37] J.C. Schindler and A. Aguirre, “Algorithms for the explicit computation of Penrose diagrams,” *Classical and Quantum Gravity* **35**, id. 105019 (2018).
- [38] K. Schwarzschild, “Über das Gravitationsfeld eines Massenpunktes nach der Einsteinschen Theorie,” *Sitzungsberichte der Königlich Preussischen Akademie der Wissenschaften*, pp. 189–196 (1916).
- [39] K. Schwarzschild, “Über das Gravitationsfeld einer Kugel aus inkompressibler Flüssigkeit nach der Einsteinschen Theorie,” *Sitzungsberichte der Königlich Preussischen Akademie der Wissenschaften*, pp. 424–434 (1916).
- [40] J.L. Synge, “The gravitational field of a particle,” *Proceedings of the Royal Irish Academy, Section A: Mathematical and Physical Sciences* **53**, pp. 83–114 (1950).
- [41] G. Szekeres, “On the singularities of a Riemannian manifold,” *Publicationes Mathematicae Debrecen* **7**, pp. 285–301 (1960).
- [42] R.M. Wald, *General Relativity*, Chicago: University of Chicago Press, 1984.
- [43] M. Walker, “Block diagrams and the extension of timelike two-surfaces,” *Journal of Mathematical Physics* **11**, pp. 2280–2286 (1970).
- [44] H. Weyl, “Zur Gravitationstheorie,” *Annalen der Physik* **54**, pp. 117–145 (1917).
- [45] A.N. Whitehead, *The Principle of Relativity with Applications to Physical Science*, London: Cambridge University Press, 1922.